Phosphorus Speciation in Atmospherically Deposited Particulate Matter and Implications for Terrestrial Ecosystem Productivity

Peggy A. O'Day[a,*,‡], Ugwumsinachi G. Nwosu[a,‡], Morgan Barnes[b], Stephen C. Hart[a], Asmeret Asefaw Berhe[a], John N. Christensen[c], and Kenneth H. Williams[c,d]

[a] Life and Environmental Sciences Department, and the Sierra Nevada Research Institute, University of California, Merced, CA 95343

[b] Environmental Systems Graduate Group, University of California, Merced, CA 95343

[c] Earth and Environmental Sciences, Lawrence Berkeley National Laboratory, Berkeley, CA 94720

[d] Rocky Mountain Biological Lab, Gothic, CO 81225

[*] correspondence to: poday@ucmerced.edu

[‡]These authors contributed equally

submitted to: *Environmental Science and Technology*

TOC Art

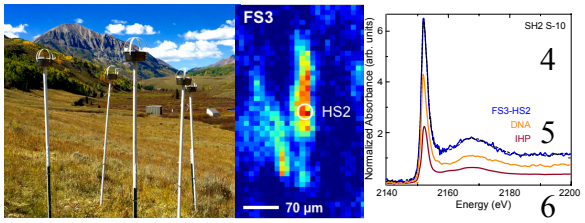
FS3
HS2
70 µm
SH2 S-10
FS3-HS2
DNA
IHP
Normalized Absorbance (arb. units)
Energy (eV)
2140
2160
2180
2200
2
4
6

ABSTRACT

Chemical forms of P in airborne particulate matter (PM) are poorly known and do not correlate with solubility or extraction measurements commonly used to infer speciation. We used P X-ray absorption near-edge structure (XANES) and ^{31}P nuclear magnetic resonance (NMR) to determine P species in PM collected at four mountain sites (Colorado and California, USA). Organic P species dominated samples from high elevations, with organic P estimated at 65–100% of total P in bulk samples by XANES and 79–88% in extracted fractions (62–84% of total P) by NMR regardless of particle size (≥ 10 μm or 1–10 μm). Phosphorus monoester and diester organic species were dominant and present in about equal proportions, with low fractions of inorganic P species. By comparison, PM from low elevation contained mixtures of organic and inorganic P, with organic P estimated at 30-60% of total P. Intercontinental PM transport determined from radiogenic lead (Pb) isotopes varied from 0-59% (mean 37%) Asian-sourced Pb at high elevation, whereas stronger regional PM inputs were found at low elevation. Airborne flux of bioavailable P to high elevation ecosystems may be twice as high as estimated by global models, which will disproportionately affect net primary productivity.

KEYWORDS: Phosphorus, particulate matter, P XANES, 31-P NMR, mountain ecosystems

INTRODUCTION

Humans have profoundly altered the biogeochemical cycling of phosphorus (P) on Earth through fossil fuel burning, intensive mining of mineral phosphate deposits, and widespread agricultural fertilization.[1] Recent studies have established that total P flux from deposition of airborne particulate matter (PM) can constitute a significant P source to ecosystem nutrient budgets in temperate climates[2, 3], following on prior work that documented the importance of airborne P deposition to tropical ecosystems.[4-6] The impact of nutrient deposition, particularly P, from regional and intercontinental sources on the trophic status of historically oligotrophic alpine lakes has been recognized.[7, 8] Global climate models suggest that net primary productivity (NPP) may increase from carbon dioxide fertilization over the next century, resulting in net increases in C storage in terrestrial ecosystems.[9] However, these potential productivity increases are dependent on the availability of growth-limiting nutrients such as nitrogen (N) and P, and nutrient limitation is one of the most uncertain factors in model prediction of terrestrial carbon storage under global change.[10]

Airborne PM (also referred to as aerosols) is a mixture of particles in solid or liquid form derived from biogenic, geogenic, and anthropogenic sources. The amount and composition of PM varies temporally and spatially, and particles undergo alteration during atmospheric transport.[11, 12] Prior studies have emphasized the importance of both natural and anthropogenic sources of atmospheric P to global biogeochemical cycles.[8, 13-19] Global estimates of airborne P emission and deposition fluxes are usually based on average concentrations measured in PM and differing assumptions about organic or inorganic P fractions, and their solubility, in particle size fractions.[8, 13, 17, 19, 20] Early studies concluded that atmospheric P on a global scale was dominated

by inorganic P as mineral particles,[13, 21] with biogenic and combustion sources comprising a relatively small fraction.(< 20%).[13, 22] More recent estimates of global P emissions suggested that anthropogenic combustion sources contribute more than 50% to the total P atmospheric budget, primarily from combustion of coal and biomass,[19] and that half of the P emitted from combustion sources may be in organic forms.[17] Most interpretations of P speciation in airborne samples are derived from measurements of total P compared with operationally defined, multi-step sequential chemical extractions designed to assess P solubility or lability in different media, and thus indirectly, potential bioavailability.[23-25] While chemical extraction methods provide information about the solubility of P-bearing species, they are not necessarily definitive regarding the chemical form or bonding environment (i.e., speciation) of P in PM, and they may introduce chemical alteration or artifacts.[26] Few studies have employed direct characterization methods to identify and quantify P species in PM. Thus, there is considerable uncertainty underlying global estimates of P flux regarding the form, potential bioavailability, and impact on ecosystem P cycling of aerially deposited PM.

Prior work examining P chemical speciation in airborne PM samples has been limited because of the analytical challenges associated with small sample mass, low P concentration, and small particle sizes. Synchrotron X-ray absorption spectroscopy (XAS) at the P K-edge, mostly as X-ray absorption near-edge structure (XANES) analysis, has been used in a few studies to characterize P speciation in PM, with estimates of relative proportions of organic and inorganic P in component mixtures varying from 0 to 100% by bulk P XANES fits.[27, 28] In the western U.S., P XANES was used to estimate Ca-P, Fe-P, and organic-P fractions in particles deposited on snow from sites in the central Rocky Mountains.[26] Particle size analysis indicated that samples

were primarily silt sized (3.9 to 63 μm) and were dominated by Ca-P and Fe-P species (68 to 92%), leading the authors to conclude that the particles originated from regional sources in the Colorado plateau.[26] In PM samples deposited in volcanic areas in northern Arizona, organic P estimated by P XANES comprised from 0 to 25% of total P.[29] To our knowledge, ^{31}P NMR spectroscopy has not been applied to the study of airborne PM, although this method has been used to characterize P species in a variety of soils and environmental samples.[30, 31]

We propose that the ecosystem impact of P from aerially deposited PM from global and regional sources depends on both the amount deposited and on P chemical speciation, which determines the mechanism and rate of P cycling once PM is incorporated into surface soils. In this study, we used XAS and NMR to identify P species and quantify mixtures in PM collected by passive sampling and filtration at two mountain watershed sites in Colorado (CO) and California (CA), USA, over an approximately one-year period. Potential sources of PM were evaluated using analysis of lead isotope ratios (in particular $^{206}Pb/^{207}Pb$ and $^{208}Pb/^{207}Pb$) and compared with a large published data set from the western United States and Asia. Lead can be emitted as a co-pollutant in industrial and urban plumes and transported as fine aerosols, with the principal fraction from 2001-2009 associated with coal combustion followed by non-ferrous ore smelting.[32] Changes in fuel use, agricultural practices, and climate change will influence PM sources and global transport, which in turn will impact P speciation and its ability to stimulate NPP, particularly in P-limited, high elevation ecosystems.

MATERIALS AND METHODS

See Supporting Information (SI) for method details.

Study Sites and Sample collection

Airborne particulate matter (PM) was collected by passive sampling at two high elevation sites (3100 m, site LS; 2800 m, site PH) in the East River Watershed, Colorado (CO-ERW) study area, and at high (2500-2700 m, site SH) and low (400 m, site SJ) elevation sites in the Southern Sierra Critical Zone Observatory (CA-SSCZO) (see Fig. S1 and Table S1 for locations and elevations). The CO-ERW sites were sampled by dry deposition (Sept.-Oct. 2016) and by snow sampling (winter, 2017), and the CA-SSCZO high elevation site was sampled twice by dry deposition (Sept.-Nov. 2016; Jul.-Sept. 2017), and once by snow sampling (winter, 2017). The low elevation site CA-SSCZO (SJ) was below the snow line and was sampled three times by dry deposition (Sept.-Oct. 2016; Jun.-Jul. 2017; Aug. 2017). Samples were collected using acid-cleaned passive collectors (25.4 cm diameter Teflon-coated pans) filled with glass beads following previously employed methods.[2] Multiple collectors were deployed on 2-m high wooden poles at each site for one to two months. Pans were retrieved, washed with DI water, and filtered in series with 10 μm (PM ≥ 10 μm) and 1 μm (PM 1–10 μm) PTFE filters (for one sample, SJ1, 0.2 μm filters were used). For snow samples, melted snow water was filtered with 10 and 1 μm PTFE filters.

Sample analysis

Elemental analysis: Elemental sample composition was determined by acid digestion of PM samples and analysis by ICP-OES (PerkinElmer Optima 5300 DV) and ICP-MS (Agilent 7500cs). Samples were digested using microwave acid digestion (Anton Paar Multiwave 3000) with aqua regia (9 mL HCl and 3 mL HNO_3 to ~10-20 mg of dried sample). Digests were diluted with ultrapure water to 4% nitric acid prior to element analysis. In addition to PM analysis, the DI water used for size filtration of PM samples was measured for dissolved total P.

121 *Phosphorus K-edge XAS:* Sized-fractioned PM samples were analyzed directly on filters by bulk
122 and microfocused XANES at beamline 14-3 at the Stanford Synchrotron Radiation Lightsource
123 (SSRL, Stanford, CA) and at the soft X-ray micro-characterization beamline (SXRMB) at the
124 Canadian Light Source (CLS, Saskatoon, Canada). Spectra were collected by mounting PM
125 filters on a P-free, double-sided carbon tape. Samples were maintained in either a He gas
126 environment or a vacuum during data collection at room temperature. Energy at the P K-edge
127 was calibrated at the P K-edge using multiple standards. A set of reference spectra consisting of
128 17 compounds or adsorbed species were used in least-squares linear combination fits (LCF) to
129 estimate P speciation in bulk samples (Fig. S4). Standards were collected for each data collection
130 run and cross-calibrated between different beamlines and runs. Fits were performed with the
131 component sum not forced to unity and only best fits within 2.5% of 100% were accepted.
132 Microfocused X-ray fluorescence (μ-XRF) maps and XANES were collected on a subset of
133 samples using a 10 μm beam size to verify P components in mixtures.
134 *Solution ^{31}P NMR:* Extractable P from PM samples was characterized by solution NMR. Sample
135 masses of 30-70 mg were extracted with 5 ml of 0.25 M NaOH and 0.05 M EDTA solution for 6
136 h, followed by centrifugation. Supernatent solutions were decanted, filtered, frozen (-18 °C) and
137 lyophilized for 24 h to concentrate extracted compounds. Freeze-dried particles were
138 reconstituted to a 0.8-1.0 ml volume with 1 M NaOH, from which samples were prepared and
139 immediately used for analysis by ^{31}P solution NMR. Spectra were acquired at 20 °C on a two-
140 channel Agilent 500 MHz ProPulse500 NMR System with a One NMR Probe and a 96-Sample
141 Robot, which operates at ^{31}P frequency of 202.4 MHz. Spectra was collected for 16 h (8600
142 scans) but scans were saved every 4 h (8600 scans) to monitor peaks over time. The instrument
143 was continuously checked with an external standard (85% phosphoric acid, 0 ppm) to correct for

144 instrumental drift. Standards (sodium phosphate, D-glucose 6-phosphate, lecithin,
145 deoxyribonucleic acid (DNA), myo-inositol hexaphosphate (myo-IHP)) were collected
146 individually and used to verify peak positions and chemical shifts.[31] Spectra were processed with
147 reference to the orthophosphate peak standardized to 6 ppm .[31, 33] Peak assignments were further
148 confirmed by spiking previously analyzed samples with orthophosphate and P standards α- and
149 β- glycerophosphate, myo-IHP, D-glucose 1-phosphate, and D-glucose 6-phosphate (Fig. S5) .
150 The residue remaining after NaOH-EDTA extraction was digested and analyzed by ICP-OES to
151 determine the amount of unextracted P by difference.
152 *Lead Isotopic Analysis:* Lead isotopic analysis was done with a Neptune Plus (Thermo-Fisher)
153 multi-collector ICP source mass spectrometer (MCICPMS) at Lawrence Berkeley National
154 Laboratory (LBNL) followed prior methods.[34, 35] Aliquots of solutions from samples dissolved
155 for total element analysis were taken to provide 10-100 ng of Pb for isotopic analysis. Matrix
156 elements were removed from the sample solution, which was then dried and resuspended in 1 ml
157 high purity 0.3 M HNO_3, from which 10% by volume was taken for determination of Pb
158 concentration. Based on this result, the remaining sample was spiked with natural Tl (NIST
159 SRM997) at ~5 ng Tl per 25 ng sample Pb. The isotopic composition of the Tl-sample Pb
160 mixture was measured on the Neptune Plus using the monitored $^{230}Tl/^{205}Tl$ ratio to correct
161 measured $^{206}Pb/^{207}Pb$ and $^{208}Pb/^{206}Pb$ for instrumental mass fractionation, along with
162 normalization to the NIST SRM981 Pb isotopic standard spiked with Tl as above. Sample
163 $^{206}Pb/^{207}Pb$ and $^{208}Pb/^{206}Pb$ were also corrected for total chemistry blank, which in most cases
164 was less than 1% of sample Pb mass. Analytical uncertainties (2σ) of the $^{206}Pb/^{207}Pb$ and
165 $^{208}Pb/^{206}Pb$ ratios were better than ±0.01 ‰ based on replicates of SRM981. The fraction of Pb in

166 PM from Asian sources was calculated using a mixing model presented by Ewing et al.[34] and
167 subsequent studies.[35-37]
168
169 **RESULTS**
170 **Elemental Analysis**
171 Bulk elemental analysis of PM showed that CO-ERW samples on average had lower P
172 concentrations compared to those from CA-SSCZO, but there was considerable variability
173 among samples (average P 30.7 ± 9.4 vs. 53.1± 19 μmol g_{PM}^{-1} or 0.951 vs. 1.64 mg g_{PM}^{-1},
174 respectively; see SI for results). The high elevation CA-SSCZO samples (SH site) had the
175 highest total P concentrations (mean 66.1 ± 15 μmol g_{PM}^{-1} or 2.05 mg g_{PM}^{-1}), with no differences
176 among samples collected by either dry deposition or as snow. Among the low elevation CA-
177 SSCZO samples, average P concentrations were lower in SJ1 and SJ3, collected in Sept.-Oct.
178 2016 and Aug. 2017, respectively, compared to SJ2, collected in Jun.-Jul. 2017. These
179 concentrations are similar to average values reported previously for CA-SSCZO sites.[2] Analysis
180 of filtrate water for total P showed concentrations ranging from below instrumental detection
181 (0.32 μmol L^{-1} or 10 μg L^{-1}) up to 65 μg L^{-1}, except for filtrate water from two low elevation
182 CA-SSCZO samples (SJ2 and SJ3), which contained 103.1 ± 1.2 μg L^{-1} and 327.6 ± 39.4 μg L^{-1}
183 P, respectively. These analyses indicated that most inorganic P in PM samples was not readily
184 water soluble over the duration of the sample filtration. Analyses of major elements showed that
185 aluminum (Al) was the most abundant element among all samples, with the highest
186 concentrations measured at the low elevation SJ site, all of which were collected by dry
187 deposition (Fig. S2). Samples at the high elevation sites were collected by either dry deposition

or snow sampling, and total element concentrations were generally lower than for SJ samples (Fig. S2 and S3).

Phosphorus K-edge XANES

Bulk XANES spectra. Estimates of P speciation in bulk PM samples from linear combination fits (LCF) of XANES reference spectra showed that high elevation CO and CA sites were dominated by organic forms of P rather than inorganic P (Fig. 1 and 2). At these sites, organic P compounds, primarily as P monoesters (fit as inositol hexakisphosphate (IHP)) and P diesters (fit as DNA or DNA adsorbed on gibbsite) species, comprised 66-100% of the XANES spectrum (see SI Table S2 for numerical results). Inorganic Ca-phosphate (as either hydroxyapatite or $CaHPO_4$), Al-phosphate (as $AlPO_4$), or adsorbed orthophosphate (as PO_4 adsorbed on gibbsite) comprised the remaining fraction(s). At the high elevation sites, no systematic differences were apparent among PM samples collected during summer and fall by dry deposition compared to PM filtered from melted snow samples (Fig. 1). Proportions of P monoester to P diester were variable across seasons and among high elevation sites. Hydroxyapatite (CaHAP) was detected as a minor component in only two of the samples from high elevation sites (PH2 and SH3, ≥ 10 μm). Both PM ≥ 10 μm and PM 1–10 μm filter samples had similar components in variable mixtures, with no obvious differences (Fig. 1 and 2).

Phosphorus speciation at the low elevation CA-SSCZO site (SJ) was more variable than at high elevation sites based on XANES fits (Fig. 2). All three dry deposition samples contained different proportions of organic and inorganic forms of P, the latter varying from 22-81% of total P. All spectra contained Ca-phosphate (as CaHAP; one spectrum had $CaHPO_4$) and often a

fraction of Al-phosphate (as $AlPO_4$ or PO_4 sorbed on gibbsite). Samples collected over one summer month (SJ3, Aug. 2017) were notable for containing a significant fraction of inorganic Fe-phosphate species (as orthophosphate sorbed on goethite or $FePO_4$) in addition to Ca-phosphate. Organic P species were a mixture of P monoesters (as IHP) and P diesters (as DNA).

*Microfocused (*μ-*) XRF and XANES.* The spatial distribution and speciation of P was studied in selected PM samples (≥ 10 μm; LS2, SH2, and SJ2) using μ-XRF and μ-XANES to examine heterogeneity and compare with bulk XANES analysis. Fluorescence mapping showed that P was distributed sparsely in PM samples with a few spots of concentrated P. In general, μ-XANES spectra collected at hot spots were mixtures of more than one P species at the scale of the beam spot (10 μm), with components similar to those identified in the bulk spectrum. Analysis of μ-XANES from the CO-ERW LS site showed evidence for P monoester and diester components either as bulk or adsorbed species, and a minor amount of inorganic P fit as adsorbed orthophosphate (Fig. 3a). Similarly, P hot spots in the high elevation CA-SSCZO (SH2) were dominated by organic P, with minor inorganic P species (Fig. 3b). Consistent with the analysis of bulk XANES spectra of the low elevation CA-SSCZO SJ site, μ-XANES of hot spots in the SJ2 sample were more variable and showed mixtures of organic and inorganic P species (Fig. 3c). Some μ-XANES spectra from SJ showed features characteristic of mineral hydroxyapatite, whereas other μ-XANES were fit with mixtures of P monoester and P diester spectra.

232 **Solution ^{31}P NMR Analysis of Extracted PM Samples**

233 A subset of samples (≥ 10 μm) were extracted by NaOH-EDTA solutions and analyzed by ^{31}P
234 solution NMR (Fig. 4). The fraction of total P extracted to solution was higher in samples from
235 high elevation CO-ERW and CA-SSCZO sites (80-89%) than from the low elevation CA-
236 SSCZO SJ site (51%; Table 1). Spectra from the high elevation LS and SH sites exhibited a
237 higher abundance of peaks associated with organic P monoester and dieseter compounds than the
238 low elevation SJ site (Fig. 4). Inorganic and organic P fractions determined by area integration of
239 chemical shift peaks identified in the NMR spectra and summation of chemical classes (Table
240 S3) showed that all of the high elevation sites were dominated by organic P compounds (66-
241 78%). The low elevation SJ site was the only site in which the fraction of inorganic P (68%) was
242 greater than organic P (Table 1). The diester region of the NMR spectrum was composed
243 primarily of DNA (~ –0.3 ppm), but there was also evidence of peaks assignable to RNA,
244 phospholipids, lipoteichoic acids, and their degradation products (Fig. 4; Table S3).[31] Peaks in
245 the P monoester region indicated the presence of IHP, α- and β- glycerophosphate, and sugar
246 phosphates (glucose 1-phosphate and glucose 6-phosphate) (Fig. S5). Among inorganic P
247 species, spectra were dominated by orthophosphate, and minor peaks were assigned to
248 pyrophosphate, doublet polyphosphates end groups, and triplet polyphosphate mid-chain groups
249 (Table S3). Inorganic polyphosphate groups contributed about 5-10% of the extractable P in all
250 samples.
251
252 Summation of chemical shift peak areas showed that P monoester compounds were more
253 abundant overall than P diester compounds. However, monoester α- and β- glycerophosphate are
254 thought to be degradation products of primary phospholipid compounds generated during

chemical extraction and NMR analysis.[38, 39] Correcting for this degradation from diester to monoester compounds shifted ratios such that P diester compounds were about twice as abundant as P monoesters at the high elevation sites, whereas monoester P compounds were still more abundant at the low elevation SJ site (Table 1).

Pb Isotope Analysis

Ratios of naturally occurring isotopes of lead (^{206}Pb, ^{207}Pb, and ^{208}Pb) in samples were measured to estimate sources of PM following prior studies of Pb fingerprinting of PM2.5 samples in the western U.S.[34-37] The measured ^{206}Pb/^{207}Pb and ^{208}Pb/^{206}Pb of the PM samples (Fig. 5) were used to calculate the fraction of Pb in the sample originating from Asian sources using the mixing model of Ewing et al.[34] (see SI, Table S4). In general, ^{206}Pb/^{207}Pb and ^{208}Pb/^{206}Pb of this study were higher than those measured in prior studies of PM samples from central California and eastern Nevada (Fig. 5). Mixing calculations showed variable inputs of Pb from Asian sources ranging from 0% to 59% among all samples, with some samples collected at the same time having similar Pb isotope ratios and others not (Table S4). For example, analysis of replicate filters (n = 5) of melted snow from CO-ERW (LS2) were tightly clustered, with the fraction of Asian Pb varying from 52-59%. In dry deposition samples collected in fall 2016 (LS1, PH1), the fraction of Asian Pb was lower (0-34%). Analyses of replicate filter samples (dry deposition, n = 4) in fall 2017 from the high elevation CA-SSCZO (SH3) site had similar fractions of Asian Pb (26-31%), whereas a snowmelt sample (SH2) had lower ^{206}Pb/^{207}Pb and ^{208}Pb/^{206}Pb ratios and a higher Asian Pb fraction (38%). Analyses of dry deposition samples from low elevation CA-SSCZO (SJ1, SJ2, and SJ3) had variable amounts of Asian Pb, even among replicate filter samples (Fig. 5, Table S4). For example, Asian Pb in SJ2 replicates (n = 4) varied from 14-52%,

whereas SJ3 replicates (n = 4) varied from 5-17% Asian Pb. However, Pb concentrations were also variable among replicates; for example SJ2 replicates ranged in Pb concentration from 24-33 ppm, with the highest concentration corresponding to the highest faction of Asian Pb (Table S4). Overall, the high elevation sites (CO and CA) had a mean estimated Asian Pb fraction of 36.8% (n = 14) and the mean from low elevation (CA) samples was 19.3% (n = 9).

DISCUSSION

Phosphorus Speciation in Deposited Particulate Matter

Spectroscopic characterization of PM samples by two independent methods, synchrotron XAS and solution ^{31}P NMR, showed that P speciation in samples from high elevation sites in CO and CA was dominated by organic P species, regardless of season or PM size (either ≥ 10 μm or between 1 – 10 μm). In contrast, the low elevation CA site had variable mixtures of different organic and inorganic P species. These results demonstrate that P in airborne PM is a spatially and temporally variable mixture of different types of P compounds that is not dominated by inorganic orthophosphate compounds or species. Furthermore, the lack of major differences in P species between the two size fractions is important for global modeling studies, which often assume P deposition rates based on particle size.[8, 15]

Bulk XANES analysis performed directly on sample filters produced a weighted distribution of all P species in a sample, while NMR analysis provided detailed identification of P species in the base-extractable fraction. The fraction of organic P was estimated at 66-100% from P XANES and species identification was corroborated by microfocused mapping and XANES spectral analysis. The fraction of total P removed by chemical extraction (62–84%) in high elevation

samples was mostly organic P. as determined by NMR (79–88%). In contrast, P species from the low elevation CA-SSCZO SJ site contained variable mixtures of total organic (30-60% by XANES) and low total extractable (51%) P that was mostly inorganic P (65%), as indicated by NMR. Samples from the SJ site had the highest fractions of crystalline P phases by XANES (fit as hydroxyapatite or $CaHPO_4$) and high fractions of adsorbed and Fe-associated orthophosphate over all periods of sample collection. Although temporal sampling was limited to about one year, no obvious differences were apparent among samples at high elevation sites collected by dry deposition over 1 to 2 months during the fall compared with melted snow samples collected at the end of winter and integrated over a longer deposition period. For all samples, PM was suspended in aqueous solution (either by washing pans or melting snow) and filtered, so any highly soluble compounds were dissolved, and the remaining less soluble material would represent particles that would be delivered to the surface soil. Comparison of speciation and extraction results indicate that organic P and adsorbed orthophosphate were more readily extracted by NaOH-EDTA than crystalline P phases, and that most organic P was extracted from bulk samples by this chemical treatment. These results agree with a prior study of PM samples using P XANES and extraction that noted a higher solubility in general for organic P compared with inorganic P fractions, but also emphasized variability among samples and poor correlation of extractable P with XANES component assignments.[27]

Estimates of the distribution of organic P species by XANES or NMR differed by method but were in general agreement. XANES fits estimated mostly higher fractions of P diester compared with P monoester, whereas uncorrected NMR results indicated that organic P was present mostly as P monoester species, with a smaller fraction of P diester distributed mostly as DNA, RNA,

and phospholipids. However, correction of estimated fractions by accounting for degradation of phospholipid diester compounds to monoester α- and β- glycerophosphate indicates slightly more diester than monoester species in most high elevation PM samples, roughly similar to the XANES results. Additional uncertainty arises from the estimation methods used for determining components in mixtures for each technique (spectral fitting for XANES; peak assignments and integrations for NMR). As discussed in prior reviews[40-42], ^{31}P NMR spectroscopy is sensitive to chemical shifts in different organic and inorganic P species and can provide more detail about individual species than P XANES, although characterization of bulk materials compared to sample extracts remains a challenge for NMR. For XANES analysis, using a large set of reference spectra (n = 17) in our analysis improved the ability to differentiate types of P species between organic and inorganic classes. Prior P XANES studies of soil and PM samples that used few P reference compound spectra in their XANES LCF analysis may have inaccurately estimated P fractions by assuming that all organically bound forms of P had a similar spectral signature. Although different types of organically bound P are spectrally similar and lack distinct features in their XANES, our data showed subtle but resolvable differences among different classes of organic P compounds, particularly between P monoeser and diester linkages, and among P monoester (phytate) bonded to metal cations, as noted in other studies.[43, 44]

Sources of Phosphorus in Particulate Matter

Analysis of Pb isotopes of PM samples indicated that seasonally variable long-range transport from Asian sources is a significant contributor of PM to both CO and CA high elevation sites in the western U.S. (up to 59% Asian Pb; mean 36.8%), but was generally lower at the low elevation CA site over all seasons (mean 19.3%). Samples from the latter site collected in August

2017 (SJ3), which had low organic P and high fractions of inorganic Fe- and Ca- associated P determined by XANES analysis, had low Asian Pb fractions (5-17%), suggesting that these inorganic P species were locally or regionally derived. Molar ratios of total P to Pb in digested PM samples varied by almost an order of magnitude (P/Pb = 127 to 1200), but there was no correlation of P/Pb with the Asian Pb fraction (Fig. S7). Prior studies of PM sourcing using Pb isotopic ratios found a median value of 29% Asian input to coastal California sites[34], and seasonally high inputs to California and the Great Basin in spring and fall.[34, 36, 37] Using Sr and Nd isotopes, Aciego et al.[2] estimated that 18-45% of PM deposited at the CA-SSCZO sites was sourced from Asia, with the remaining fraction derived regionally from the California Central Valley. At two high elevation CA-SSCZO sites, it was estimated that about 10-20% of PM input in July was derived from Asia, whereas about 20-40% was Asian-sourced in October.[45] This study and others estimate that, on average annually, about one third of the PM deposited in the western US is sourced from the Asian continent, although inputs are spatially and temporally variable.[34, 36, 37] Aerosols from Asia are a mixture of anthropogenic combustion products and geogenic particles from desert regions.[36, 46] Our data are in agreement with these prior studies that demonstrated a mix of Asian and local sources for PM, and similarly showed variability among samples collected over the same time interval in the fraction of PM derived from local or regional sources compared to intercontinental transport.

Previous studies of global P transport in airborne PM classified sources of P as mostly geogenic dust, biomass burning (including fossil fuels, biofuels, and wildland fires), and primary biogenic particles (e.g., vegetation, microorganisms, decomposed biomolecules), with minor inputs from industrial and mining emissions, and volcanoes.[8, 13, 17, 19, 20] One prior study suggested that

370 bacteria were a dominant source of soluble organic P in marine aerosols from the Mediterranean
371 Sea[27], while another estimated that half of the P emitted from combustion sources may be in
372 organic forms.[17] Inorganic P species have been attributed to local or regional sources of aeolian
373 geogenic dust.[26, 28] We were not able to distinguish whether organic P in our samples comes from
374 primary biogenic or fossil organic (combustion) sources, or a mixture of both. Regarding the
375 inorganic P fraction in our PM samples, we observed evidence for orthophosphate adsorbed to
376 Al- or Fe-oxide phases rather than, or in addition to, crystalline phosphate phases such
377 hydroxyapatite in high elevation samples. Adsorbed orthophosphate may have been derived from
378 the breakdown of either organic compounds or primary phosphate minerals either at the source
379 (combustion, soil) or as a result of atmospheric alteration, especially in acidic conditions.[12, 20, 47]
380
381 **Implications for Ecosystem Productivity**
382 As an essential plant nutrient, P bioavailability can control the rate of non-agricultural, P-limited
383 ecosystems to sequester carbon.[10] Classical models of pedogenesis hold that weathering of
384 inorganic P in soils is a dominant source of P for biosysnthesis, but in recent decades the
385 importance of organically bound P in ecosystem nutrient regulation has emerged.[48, 49] Studies of
386 soil and aquatic environments suggest that the most rapidly exchanging pool of P is associated
387 with degradation of labile organic matter.[49, 50] Short-term rates of organic P conversion to
388 dissolved orthophosphate (gross mineralization) estimated from radioactive isotope dilution
389 experiments are fast, generally in the range of 0.1-2.5 mg P kg_{soil}^{-1} d^{-1} and as high as 12.6 mg P
390 kg_{soil}^{-1} d^{-1}, and are thought to be mostly controlled by biological and enzymatic processes.[51] For
391 example, a key step in the conversion of organic P species to orthophosphate is hydrolysis of the
392 P-O-C ester linkage in P diesters and terminal P monoesters catalyzed by biologically produced

393 phosphatase enzymes.[52, 53] With soil development, some P may partition to occluded or protected
394 pools that are relatively non-bioavailable, with decomposition rates orders of magnitude slower
395 than fast-cycling C and nutrient pools.[54, 55]
396
397 Our spectroscopic evidence showed that, regardless of particle size or season of deposition,
398 aerially deposited PM is dominated at high elevation sites by organic P in monoester and diester
399 molecular forms in about equal proportions, not inorganic P in primary mineral phases such as
400 apatite. Orthophosphate diester compounds are generally more soluble and undergo degradation
401 by hydrolysis more readily than monoester IHP, and thus are thought to be more labile and
402 bioavailable than IHP in the soil environment.[39, 48, 51, 56] However, quantitative measurements of
403 reaction rates for particular compound classes are lacking. Some studies have suggested that
404 adsorption of organic P compounds reduces P bioavailability, but other studies argue that
405 adsorption on mineral surfaces may promote hydrolysis and enhance bioavailability.[57-59]
406 Phosphate apatite minerals generally have low solubilities and slow kinetic rates of dissolution
407 that are pH-dependent[60, 61], and their bioavailability in soils will depend on factors such as
408 particle size and surface area, degree of crystallinity, and local solution pH and cation
409 concentration. Plants and microorganisms take up orthophosphate ($H_{3-x}PO_4^{x-}$), but since
410 dissolved concentrations in soils are generally very low, organisms have multiple strategies for
411 solubilizing P from both organic and inorganic pools through the secretion of organic acids,
412 carboxylate anions, and organic metabolites.[50, 62] Overall, our results suggest that, at high
413 elevation sites, the dominance of reactive organic P chemical species and non-crystalline
414 inorganic P, together with small particle sizes of airborne PM, should result in P deposition that
415 is rapidly assimilated by biological soil processes.

Recent global modeling estimates of total P emissions to the atmosphere range from about 1.3 to 3.7 Tg P yr^{-1} [19, 20, 22], but estimates of the soluble or bioavailable P fractions vary depending on model assumptions. Most models rely on a combination of factors, including size fraction distributions, bulk elemental composition, elemental ratios, and operational solubility measurements of PM, together with atmospheric transport modeling, to estimate P depositional fluxes and soluble fractions.[8, 13, 17] For example, Myriokefalitakis et al.[20] estimated that fractions deposited as soluble P (0.45 Tg P yr^{-1}) or bioavailable P (0.47 Tg P yr^{-1}) were about 35% of the total P depositional flux (1.3 Tg P yr^{-1}), and more than 80% of total P emissions were derived from "mineral" P sources. In contrast, Wang et al.[19] estimated a higher global total P annual emission (3.5 Tg P yr^{-1}) based on higher P contributions (over 50%) from fossil fuel and biomass combustion sources. It has been assumed that the P fraction derived from combustion sources is more soluble and thus more bioavailable in the oceans[13, 20] and potentially in tropical forests[25], although other studies have shown more complicated relationships between P solubility as measured by water or chemical extractions and bioavailability.[23, 63] Our determination of organic P species comprising 60-100% of total P in PM at high elevation sites suggests that the fraction of soluble or bioavailable P may be twice as high as estimated in current global cycling models (30-50%).[19, 20, 22]

As ecosystem NPP and organic matter cycling rates increase with climate warming, the amount and speciation of P in PM from both regional and intercontinental sources will have an increasingly important effect on P-limited ecosystems. This is particularly true for mountain regions where up-gradient shifts of vegetation zones with warming are already occurring, but

changes in nutrient availability (particularly N and P) are poorly known and may constrain these vegetation range shifts.[64] On both a global and regional scale, P emission fluxes to the atmosphere are likely to increase, driven by combustion of fuel and biomass, agricultural practices and land management (e.g., deforestation, grazing), increasing intensity and frequency of droughts, and other anthropogenic forcings if current trends continue.[19, 25] In order to accurately predict impacts and design effective mitigation policies, ecosystem models will need to incorporate both total fluxes and species-based cycling rates of P into future projections. Given the P species in deposited PM identified here, we suggest that airborne P flux to high elevation regions that is soluble or bioavailable may be twice as high as estimated by current global models. This depositional flux will have a disproprotionate effect on NPP by supplying a high fraction of reactive P species that will cycle rapidly when incorporated into surface soils.

ASSOCIATED CONTENT

Supporting Information

Supporting information is available free of charge at http://pubs.acs.org.

Detailed descriptions of materials and methods; table of sample locations and sampling periods; figures of total element concentrations, P XANES reference spectra, chemical shift regions and standards for ^{31}P NMR spectra, illustration of calculation for Asian Pb fraction, and percent Asian Pb as a function of molar P/Pb. Tables with fit results for bulk XANES spectra, NMR chemical shift assignments for standards, and Pb concentrations, isotope ratios, and Asian fraction.

AUTHOR INFORMATION

Corresponding author

*E-mail: poday@ucmerced.edu

Notes

The authors declare no competing financial interest.

ACKNOWLEDGEMENTS

This research was funded by the Subsurface Biogeochemical Research Program (DE-SC0016479), U.S. Department of Energy. Portions of this research were carried out at the Stanford Synchrotron Radiation Lightsource, a national user facility operated by Stanford University on behalf of the U.S. Department of Energy, and at the Canadian Light Source, supported by the Canada Foundation for Innovation, Natural Sciences and Engineering Research Council of Canada, the University of Saskatchewan, the Government of Saskatchewan, Western Economic Diversification Canada, the National Research Council Canada, and the Canadian Institutes of Health Research. Field sample collection in Colorado and Pb isotope analyses were supported as part of the Watershed Function Scientific Focus Area at LBNL funded by the U.S. Department of Energy under Award Number DE-AC02-05CH11231. We thank Ben Lash, Erin Stacy, and Melissa Thaw for assistance at the CA-SSCZO (supported by EAR-0725097, 1239521, and 1331939) and to Dave Rice and Fernanda Santos for help with NMR analysis. Barbara Cade-Menun provided valuable advice on NMR. The UC Merced Environmental Analytical Laboratory supported analytical instrumentation.

REFERENCES

(1) Cordell, D.; White, S., Life's Bottleneck: Sustaining the World's Phosphorus for a Food Secure Future. In *Annual Review of Environment and Resources, Vol 39*, Gadgil, A.; Liverman, D. M., Eds. Annual Reviews: Palo Alto, 2014; Vol. 39, pp 161-+.

(2) Aciego, S. M.; Riebe, C. S.; Hart, S. C.; Blakowski, M. A.; Carey, C. J.; Aarons, S. M.; Dove, N. C.; Botthoff, J. K.; Sims, K. W. W.; Aronson, E. L., Dust outpaces bedrock in nutrient supply to montane forest ecosystems. *Nature Comm.* **2017,** *8*, 10.

(3) Arvin, L. J.; Riebe, C. S.; Aciego, S. M.; Blakowski, M. A., Global patterns of dust and bedrock nutrient supply to montane ecosystems. *Sci. Adv.* **2017,** *3*, (12).

(4) Chadwick, O. A.; Derry, L. A.; Vitousek, P. M.; Huebert, B. J.; Hedin, L. O., Changing sources of nutrients during four million years of ecosystem development. *Nature* **1999,** *397*, (6719), 491-497.

(5) Pett-Ridge, J. C., Contributions of dust to phosphorus cycling in tropical forests of the Luquillo Mountains, Puerto Rico. *Biogeochem.* **2009,** *94*, (1), 63-80.

(6) Yu, H. B.; Chin, M.; Yuan, T. L.; Bian, H. S.; Remer, L. A.; Prospero, J. M.; Omar, A.; Winker, D.; Yang, Y. K.; Zhang, Y.; Zhang, Z. B.; Zhao, C., The fertilizing role of African dust in the Amazon rainforest: A first multiyear assessment based on data from Cloud-Aerosol Lidar and Infrared Pathfinder Satellite Observations. *Geophys. Res. Lett.* **2015,** *42*, (6), 1984-1991.

(7) Homyak, P. M.; Sickman, J. O.; Melack, J. M., Pools, transformations, and sources of P in high-elevation soils: Implications for nutrient transfer to Sierra Nevada lakes. *Geoderma* **2014,** *217*, 65-73.

(8) Brahney, J.; Mahowald, N.; Ward, D. S.; Ballantyne, A. P.; Neff, J. C., Is atmospheric phosphorus pollution altering global alpine Lake stoichiometry? *Glob. Biogeochem. Cycle* **2015,** *29*, (9), 1369-1383.

(9) Todd-Brown, K. E. O.; Randerson, J. T.; Hopkins, F.; Arora, V.; Hajima, T.; Jones, C.; Shevliakova, E.; Tjiputra, J.; Volodin, E.; Wu, T.; Zhang, Q.; Allison, S. D., Changes in soil organic carbon storage predicted by Earth system models during the 21st century. *Biogeosciences* **2014,** *11*, (8), 2341-2356.

(10) Wieder, W. R.; Cleveland, C. C.; Smith, W. K.; Todd-Brown, K., Future productivity and carbon storage limited by terrestrial nutrient availability. *Nature Geosci.* **2015,** *8*, (6), 441-U435.

(11) Perlwitz, J. P.; Garcia-Pando, C. P.; Miller, R. L., Predicting the mineral composition of dust aerosols - Part 1: Representing key processes. *Atmos. Chem. Phys.* **2015,** *15*, (20), 11593-11627.

(12) Stockdale, A.; Krom, M. D.; Mortimer, R. J. G.; Benning, L. G.; Carslaw, K. S.; Herbert, R. J.; Shi, Z. B.; Myriokefalitakis, S.; Kanakidou, M.; Nenes, A., Understanding the nature of atmospheric acid processing of mineral dusts in supplying bioavailable phosphorus to the oceans. *Proc. Natl. Acad. Sci. U. S. A.* **2016,** *113*, (51), 14639-14644.

(13) Mahowald, N.; Jickells, T. D.; Baker, A. R.; Artaxo, P.; Benitez-Nelson, C. R.; Bergametti, G.; Bond, T. C.; Chen, Y.; Cohen, D. D.; Herut, B.; Kubilay, N.; Losno, R.; Luo, C.; Maenhaut, W.; McGee, K. A.; Okin, G. S.; Siefert, R. L.; Tsukuda, S., Global distribution of atmospheric phosphorus sources, concentrations and deposition rates, and anthropogenic impacts. *Glob. Biogeochem. Cycle* **2008,** *22*, (4).

(14) Okin, G. S.; Mahowald, N.; Chadwick, O. A.; Artaxo, P., Impact of desert dust on the biogeochemistry of phosphorus in terrestrial ecosystems. *Glob. Biogeochem. Cycle* **2004,** *18*, (2).

(15) Neff, J. C.; Ballantyne, A. P.; Farmer, G. L.; Mahowald, N. M.; Conroy, J. L.; Landry, C. C.; Overpeck, J. T.; Painter, T. H.; Lawrence, C. R.; Reynolds, R. L., Increasing eolian dust deposition in the western United States linked to human activity. *Nature Geosci.* **2008,** *1*, (3), 189-195.
(16) Mahowald, N., Aerosol Indirect Effect on Biogeochemical Cycles and Climate. *Science* **2011,** *334*, (6057), 794-796.
(17) Kanakidou, M.; Duce, R. A.; Prospero, J. M.; Baker, A. R.; Benitez-Nelson, C.; Dentener, F. J.; Hunter, K. A.; Liss, P. S.; Mahowald, N.; Okin, G. S.; Sarin, M.; Tsigaridis, K.; Uematsu, M.; Zamora, L. M.; Zhu, T., Atmospheric fluxes of organic N and P to the global ocean. *Glob. Biogeochem. Cycle* **2012,** *26*.
(18) Boyle, J. F.; Chiverrell, R. C.; Norton, S. A.; Plater, A. J., A leaky model of long-term soil phosphorus dynamics. *Glob. Biogeochem. Cycle* **2013,** *27*, (2), 516-525.
(19) Wang, R.; Balkanski, Y.; Boucher, O.; Ciais, P.; Penuelas, J.; Tao, S., Significant contribution of combustion-related emissions to the atmospheric phosphorus budget. *Nature Geosci.* **2015,** *8*, (1), 48-54.
(20) Myriokefalitakis, S.; Nenes, A.; Baker, A. R.; Mihalopoulos, N.; Kanakidou, M., Bioavailable atmospheric phosphorous supply to the global ocean: a 3-D global modeling study. *Biogeosciences* **2016,** *13*, (24), 6519-6543.
(21) Graham, W. F.; Duce, R. A., Atmospheric pathways of the phosphorus cycle. *Geochim. Cosmochim. Acta* **1979,** *43*, (8), 1195-1208.
(22) Tipping, E.; Benham, S.; Boyle, J. F.; Crow, P.; Davies, J.; Fischer, U.; Guyatt, H.; Helliwell, R.; Jackson-Blake, L.; Lawlor, A. J.; Monteith, D. T.; Rowe, E. C.; Toberman, H., Atmospheric deposition of phosphorus to land and freshwater. *Environ. Sci. Process. Impac.* **2014,** *16*, (7), 1608-1617.
(23) Anderson, L. D.; Faul, K. L.; Paytan, A., Phosphorus associations in aerosols: What can they tell us about P bioavailability? *Mar. Chem.* **2010,** *120*, (1-4), 44-56.
(24) Gross, A.; Goren, T.; Pio, C.; Cardoso, J.; Tirosh, O.; Todd, M. C.; Rosenfeld, D.; Weiner, T.; Custodio, D.; Angert, A., Variability in Sources and Concentrations of Saharan Dust Phosphorus over the Atlantic Ocean. *Environ. Sci. Technol. Lett.* **2015,** *2*, (2), 31-37.
(25) Barkley, A. E.; Prospero, J. M.; Mahowald, N.; Hamilton, D. S.; Popendorf, K. J.; Oehlert, A. M.; Pourmand, A.; Gatineau, A.; Panechou-Pulcherie, K.; Blackwelder, P.; Gaston, C. J., African biomass burning is a substantial source of phosphorus deposition to the Amazon, Tropical Atlantic Ocean, and Southern Ocean. *Proc. Natl. Acad. Sci. U. S. A.* **2019,** *116*, (33), 16216-16221.
(26) Zhang, Z.; Goldstein, H. L.; Reynolds, R. L.; Hu, Y.; Wang, X.; Zhu, M., Phosphorus Speciation and Solubility in Aeolian Dust Deposited in the Interior American West. *Environ. Sci. Technol.* **2018,** *52*, (5), 2658-2667.
(27) Longo, A. F.; Ingall, E. D.; Diaz, J. M.; Oakes, M.; King, L. E.; Nenes, A.; Mihalopoulos, N.; Violaki, K.; Avila, A.; Benitez-Nelson, C. R.; Brandes, J.; McNulty, I.; Vine, D. J., P-NEXFS analysis of aerosol phosphorus delivered to the Mediterranean Sea. *Geophys. Res. Lett.* **2014,** *41*, (11), 4043-4049.
(28) Hudson-Edwards, K. A.; Bristow, C. S.; Cibin, G.; Mason, G.; Peacock, C. L., Solid-phase phosphorus speciation in Saharan Bodele Depression dusts and source sediments. *Chem. Geol.* **2014,** *384*, 16-26.

(29) Gu, C.; Hart, S. C.; Turner, B. L.; Hu, Y.; Meng, Y.; Zhu, M., Aeolian dust deposition and the perturbation of phosphorus transformations during long-term ecosystem development in a cool, semi-arid environment. *Geochim. Cosmochim. Acta* **2019,** *246*, 498-514.
(30) Cade-Menun, B.; Liu, C. W., Solution Phosphorus-31 Nuclear Magnetic Resonance Spectroscopy of Soils from 2005 to 2013: A Review of Sample Preparation and Experimental Parameters. *Soil Sci. Soc. Am. J.* **2014,** *78*, (1), 19-37.
(31) Cade-Menun, B. J., Improved peak identification in P-31-NMR spectra of environmental samples with a standardized method and peak library. *Geoderma* **2015,** *257*, 102-114.
(32) Li, Q.; Cheng, H. G.; Zhou, T.; Lin, C. Y.; Guo, S., The estimated atmospheric lead emissions in China, 1990-2009. *Atmos. Environ.* **2012,** *60*, 1-8.
(33) Feng, W.; Zhu, Y.; Wu, F.; He, Z.; Zhang, C.; Giesy, J. P., Forms and Lability of Phosphorus in Algae and Aquatic Macrophytes Characterized by Solution 31P NMR Coupled with Enzymatic Hydrolysis. *Sci. Rep.* **2016,** *6*, 37164.
(34) Ewing, S. A.; Christensen, J. N.; Brown, S. T.; Vancuren, R. A.; Cliff, S. S.; Depaolo, D. J., Pb Isotopes as an Indicator of the Asian Contribution to Particulate Air Pollution in Urban California. *Environ. Sci. Technol.* **2010,** *44*, (23), 8911-8916.
(35) Christensen, J. N.; Weiss-Penzias, P.; Fine, R.; McDade, C. E.; Trzepla, K.; Brown, S. T.; Gustin, M. S., Unraveling the sources of ground level ozone in the Intermountain Western United States using Pb isotopes. *Sci. Total Environ.* **2015,** *530*, 519-525.
(36) Asher, E. C.; Christensen, J. N.; Post, A.; Perry, K.; Cliff, S. S.; Zhao, Y. J.; Trousdell, J.; Faloona, I., The Transport of Asian Dust and Combustion Aerosols and Associated Ozone to North America as Observed From a Mountaintop Monitoring Site in the California Coast Range. *J. Geophys. Res., Atmos.* **2018,** *123*, (10), 5667-5680.
(37) Pierce, A. M.; Gustin, M. S.; Christensen, J. N.; Loria-Salazar, S. M., Use of multiple tools including lead isotopes to decipher sources of ozone and reactive mercury to urban and rural locations in Nevada, USA. *Sci. Total Environ.* **2018,** *615*, 1411-1427.
(38) Doolette, A. L.; Smernik, R. J.; Dougherty, W. J., Spiking Improved Solution Phosphorus-31 Nuclear Magnetic Resonance Identification of Soil Phosphorus Compounds. *Soil Sci. Soc. Am. J.* **2009,** *73*, (3), 919-927.
(39) Schneider, K. D.; Cade-Menun, B. J.; Lynch, D. H.; Voroney, R. P., Soil Phosphorus Forms from Organic and Conventional Forage Fields. *Soil Sci. Soc. Am. J.* **2016,** *80*, (2), 328-340.
(40) Cade-Menun, B. J., Using phosphorus-31 nuclear magnetic resonance spectroscopy to characterize organic phosphorus in environmental samples. In *Organic Phosphorus in the Environment*, Turner, B. L.; Frossard, E.; Baldwin, D. S., Eds. CABI Publishing: Wallingford, Oxon, GBR, 2004; pp 21-44.
(41) Cade-Menun, B. J., Characterizing phosphorus in environmental and agricultural samples by P-31 nuclear magnetic resonance spectroscopy. *Talanta* **2005,** *66*, (2), 359-371.
(42) Doolette, A. L.; Smernik, R. J., Soil Organic Phosphorus Speciation Using Spectroscopic Techniques. In *Phosphorus in Action: Biological Processes in Soil Phosphorus Cycling*, Bunemann, E. K.; Oberson, A.; Frossard, E., Eds. 2011; Vol. 26, pp 3-36.
(43) Hesterberg, D., Chapter 11 - Macroscale Chemical Properties and X-Ray Absorption Spectroscopy of Soil Phosphorus. In *Developments in Soil Science*, Balwant, S.; Markus, G., Eds. Elsevier: 2010; Vol. Volume 34, pp 313-356.
(44) Prietzel, J.; Harrington, G.; Hausler, W.; Heister, K.; Werner, F.; Klysubun, W., Reference spectra of important adsorbed organic and inorganic phosphate binding forms for soil

617 P speciation using synchrotron-based K-edge XANES spectroscopy. *J. Synch. Rad.* **2016,** *23*,
618 (2), 532-544.
619 (45) Aarons, S. M.; Arvin, L. J.; Aciego, S. M.; Riebe, C. S.; Johnson, K. R.; Blakowski, M.
620 A.; Koornneef, J. M.; Hart, S. C.; Barnes, M. E.; Dove, N.; Botthoff, J. K.; Maltz, M.; Aronson,
621 E. L., Competing droughts affect dust delivery to Sierra Nevada. *Aeolian Res.* **2019,** *in press*.
622 (46) Brock, C. A.; Hudson, P. K.; Lovejoy, E. R.; Sullivan, A.; Nowak, J. B.; Huey, L. G.;
623 Cooper, O. R.; Cziczo, D. J.; de Gouw, J.; Fehsenfeld, F. C.; Holloway, J. S.; Hubler, G.;
624 Lafleur, B. G.; Murphy, D. M.; Neuman, J. A.; Nicks, D. K.; Orsini, D. A.; Parrish, D. D.;
625 Ryerson, T. B.; Tanner, D. J.; Warneke, C.; Weber, R. J.; Wilson, J. C., Particle characteristics
626 following cloud-modified transport from Asia to North America. *J. Geophys. Res., Atmos.* **2004,**
627 *109*, (D23), 17.
628 (47) Nenes, A.; Krom, M. D.; Mihalopoulos, N.; Van Cappellen, P.; Shi, Z.; Bougiatioti, A.;
629 Zarmpas, P.; Herut, B., Atmospheric acidification of mineral aerosols: a source of bioavailable
630 phosphorus for the oceans. *Atmos. Chem. Phys.* **2011,** *11*, (13), 6265-6272.
631 (48) Condron, L. M.; Turner, B. L.; Cade-Menun, B. J., Chemistry and Dynamics of Soil
632 Organic Phosphorus. In *Phosphorus: Agriculture and the Environment*, Sims, J. T.; Sharpley, A.
633 N., Eds. ASA, CSSA, and SSSA: Madison, WI, 2005; Vol. Agronomy Monograph 46, pp 87-
634 121.
635 (49) Baldwin, D. S., Organic phosphorus in the aquatic environment. *Environ. Chem.* **2013,**
636 *10*, (6), 439-454.
637 (50) Jansa, J.; Finlay, R.; Wallander, H.; Smith, F. A.; Smith, S. E., Role of Mycorrhizal
638 Symbioses in Phosphorus Cycling. In *Phosphorus in Action: Biological Processes in Soil*
639 *Phosphorus Cycling*, Bunemann, E. K.; Oberson, A.; Frossard, E., Eds. 2011; Vol. 26, pp 137-
640 168.
641 (51) Bunemann, E. K., Assessment of gross and net mineralization rates of soil organic
642 phosphorus - A review. *Soil Biol. Biochem.* **2015,** *89*, 82-98.
643 (52) Quiquampoix, H.; Mousain, D., Enzymatic hydrolysis of organic phosphorus. In *Organic*
644 *Phosphorus in the Environment*, Turner, B. L.; Frossard, E.; Baldwin, D. S., Eds. CABI
645 Publishing: Wallingford, Oxon, GBR, 2004; pp 89-112.
646 (53) Nannipieri, P.; Giagnoni, L.; Landi, L.; Renella, G., Role of Phosphatase Enzymes in
647 Soil. In *Phosphorus in Action: Biological Processes in Soil Phosphorus Cycling*, Bunemann, E.
648 K.; Oberson, A.; Frossard, E., Eds. 2011; Vol. 26, pp 215-243.
649 (54) Parton, W. J.; Stewart, J. W. B.; Cole, C. V., Dynamics of C, N, P and S in grassland
650 soils: a model. *Biogeochem.* **1988,** *5*, (1), 109-131.
651 (55) Fatichi, S.; Manzoni, S.; Or, D.; Paschalis, A., A Mechanistic Model of Microbially
652 Mediated Soil Biogeochemical Processes: A Reality Check. *Glob. Biogeochem. Cycle* **2019,** *33*,
653 (6), 620-648.
654 (56) Darch, T.; Blackwell, M. S. A.; Hawkins, J. M. B.; Haygarth, P. M.; Chadwick, D., A
655 Meta-Analysis of Organic and Inorganic Phosphorus in Organic Fertilizers, Soils, and Water:
656 Implications for Water Quality. *Crit. Rev. Environ. Sci. Technol.* **2014,** *44*, (19), 2172-2202.
657 (57) Olsson, R.; Giesler, R.; Loring, J. S.; Persson, P., Adsorption, Desorption, and Surface-
658 Promoted Hydrolysis of Glucose-1-Phosphate in Aqueous Goethite (alpha-FeOOH) Suspensions.
659 *Langmuir* **2010,** *26*, (24), 18760-18770.
660 (58) Olsson, R.; Giesler, R.; Loring, J. S.; Persson, P., Enzymatic Hydrolysis of Organic
661 Phosphates Adsorbed on Mineral Surfaces. *Environ. Sci. Technol.* **2012,** *46*, (1), 285-291.

(59) Baldwin, D. S.; Howitt, J. A.; Beattie, J. K., Abiotic degradation of organic phosphorus compounds in the environment. In *Organic Phosphorus in the Environment*, Turner, B. L.; Frossard, E.; Baldwin, D. S., Eds. CABI Publishing: Wallingford, Oxon, GBR, 2004; pp 75-88.
(60) Drouet, C., A comprehensive guide to experimental and predicted thermodynamic properties of phosphate apatite minerals in view of applicative purposes. *J. Chem. Thermo.* **2015,** *81*, 143-159.
(61) Oelkers, E. H.; Valsami-Jones, E.; Roncal-Herrero, T., Phosphate mineral reactivity: from global cycles to sustainable development. *Mineral. Mag.* **2008,** *72*, (1), 337-340.
(62) Jones, D. L.; Oburger, E., Solubilization of Phosphorus by Soil Microorganisms. In *Phosphorus in Action: Biological Processes in Soil Phosphorus Cycling*, Bunemann, E. K.; Oberson, A.; Frossard, E., Eds. 2011; Vol. 26, pp 169-198.
(63) Li, B.; Brett, M. T., The influence of dissolved phosphorus molecular form on recalcitrance and bioavailability. *Environ. Pollut.* **2013,** *182*, 37-44.
(64) Hagedorn, F.; Gavazov, K.; Alexander, J. M., Above- and belowground linkages shape responses of mountain vegetation to climate change. *Science* **2019,** *365*, (6458), 1119.
(65) Jones, C. E.; Halliday, A. N.; Rea, D. K.; Owen, R. M., Eolian inputs of lead to the North Pacific. *Geochim. Cosmochim. Acta* **2000,** *64*, (8), 1405-1416.
(66) Tan, M. G.; Zhang, G. L.; Li, X. L.; Zhang, Y. X.; Yue, W. S.; Chen, J. M.; Wang, Y. S.; Li, A. G.; Li, Y.; Zhang, Y. M.; Shan, Z. C., Comprehensive study of lead pollution in Shanghai by multiple techniques. *Anal. Chem.* **2006,** *78*, (23), 8044-8050.
(67) Diaz-Somoano, M.; Kylander, M. E.; Lopez-Anton, M. A.; Suarez-Ruiz, I.; Martinez-Tarazona, M. R.; Ferrat, M.; Kober, B.; Weiss, D. J., Stable Lead Isotope Compositions In Selected Coals From Around The World And Implications For Present Day Aerosol Source Tracing. *Environ. Sci. Technol.* **2009,** *43*, (4), 1078-1085.

A. CO-ERW PH

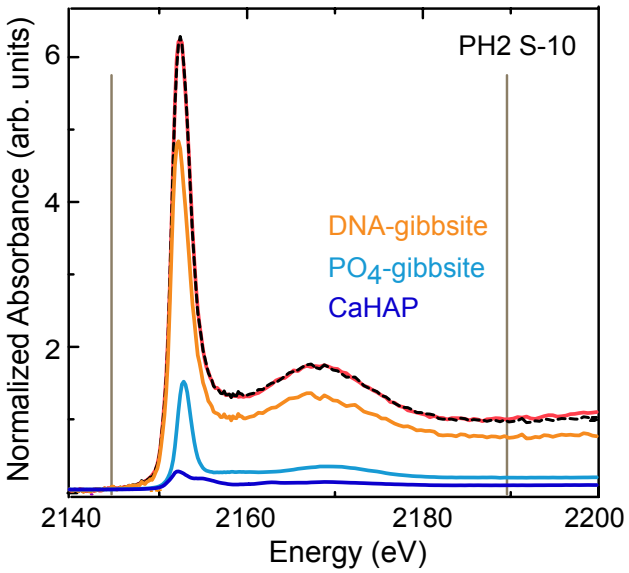

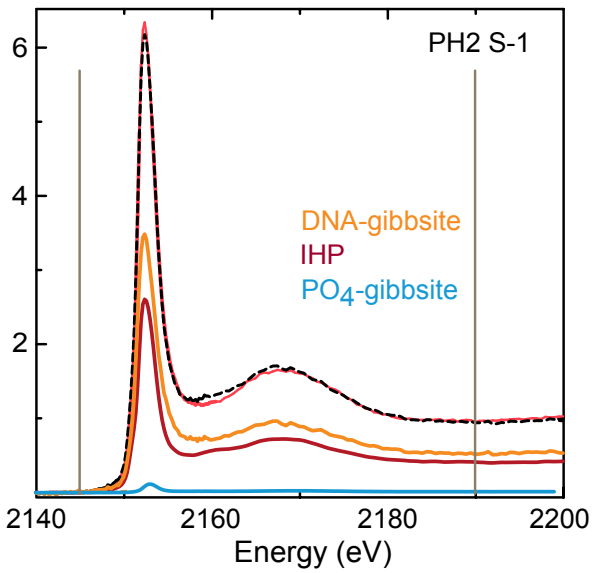

B. CA-SSCZO SH

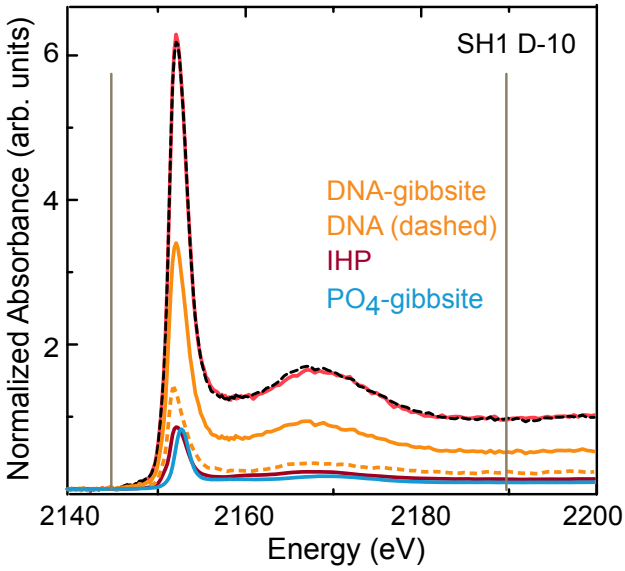

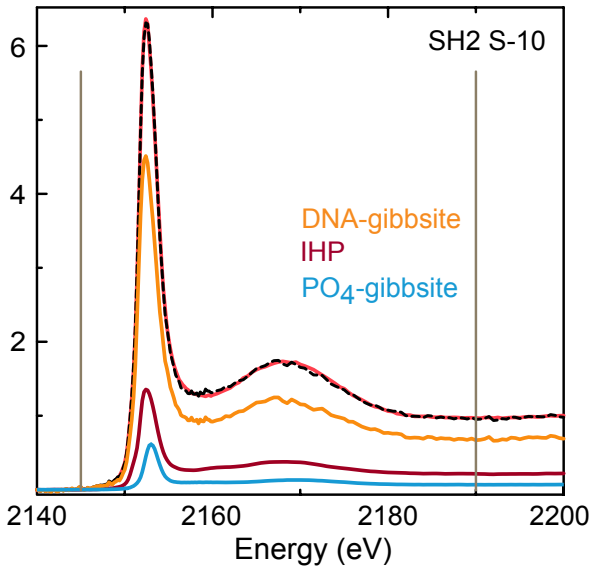

C. CA-SSCZO SJ

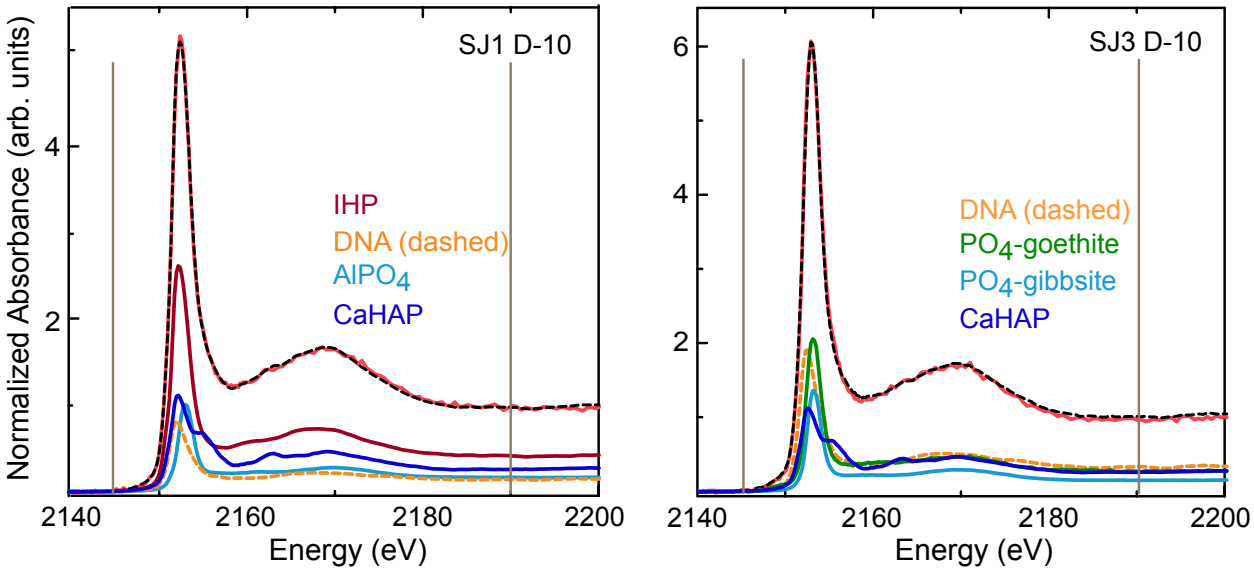

Figure 1. Phosphorus K-edge XANES of bulk particulate matter samples showing data (solid red line), linear combination best fit (dashed black line), and spectral deconvolutions of reference compounds (colored lines). A. High elevation CO samples (PH site) comparing size fractions (10 and 1 μm filters); B. High elevation CA samples (SH site) comparing dry (D) and snow (S) samples (10 μm filters); C. Low elevation CA samples (SJ site) comparing annual differences (Sept.-Oct. 2016 and Aug. 2017; 10 μm filters). Reference spectra: Inositol hexakisphosphate, Na salt (IHP); deoxyribonucleic acid (DNA); and DNA adsorbed on gibbsite (DNA-gibbsite); Ca hydroxyapatite (CaHAP), PO_4 adsorbed on gibbsite ($Al(OH)_3$; PO_4-gibbsite), and PO_4 adsorbed on goethite (FeOOH; PO_4-goethite).

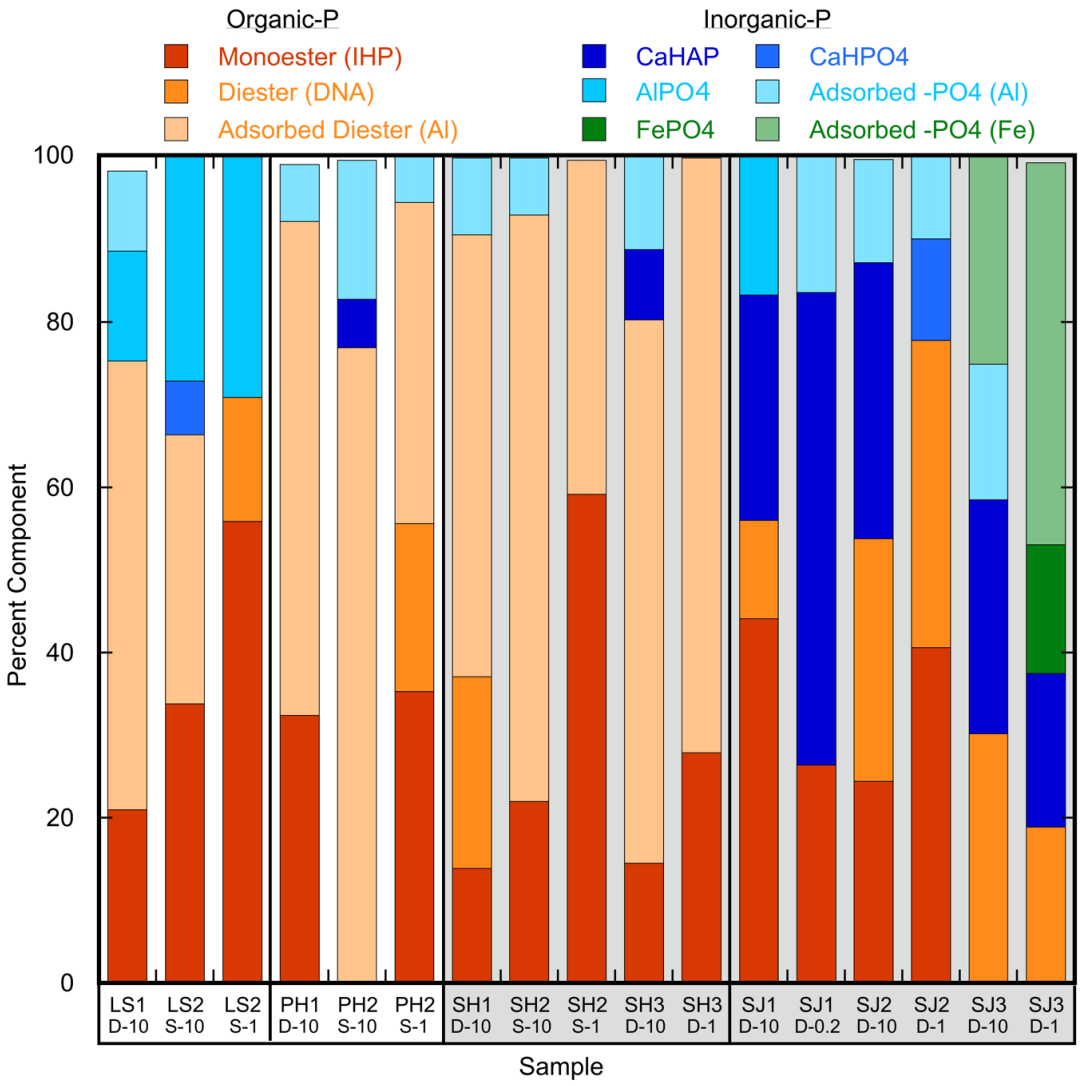

Figure 2. Summary of linear combination fits of phosphorus K-edge XANES spectra of bulk particulate matter samples using reference compound spectra (component sum not normalized; see SI for analysis details). Sites: LS, PH – high elevation CO-ERW; SH – high elevation CA-SSCZO; SJ – low elevation CA-SSCZO. Sample types: D – dry; S – snow. Filter size: 10, 1, or 0.2 μm. Numerical fit results for bulk XANES spectra reported in Table S2.

A. CO-ERW LS2 S-10

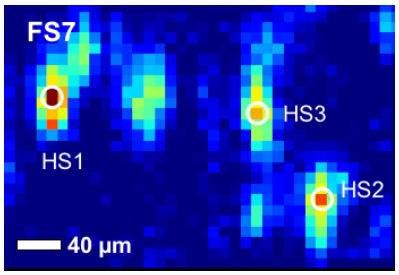

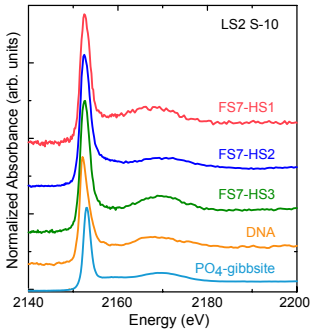

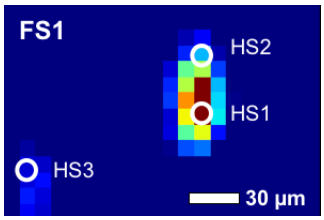

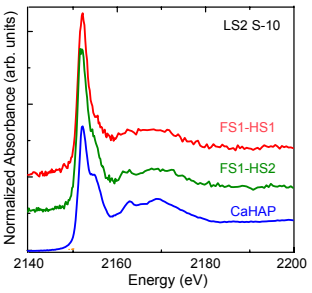

B. CA-SSCZO SH2 S-10

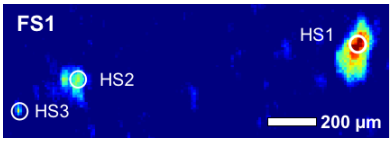

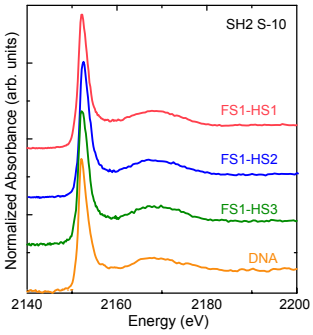

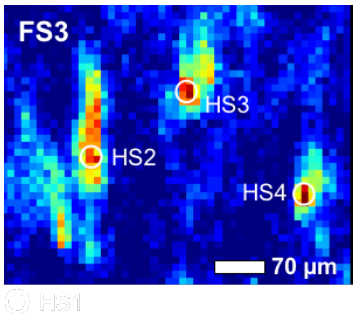

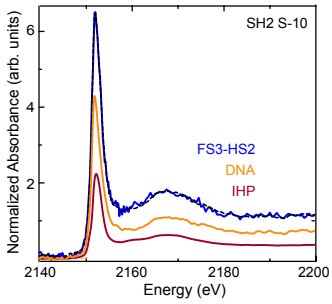

C. CA-SSCZO SJ2 D-10

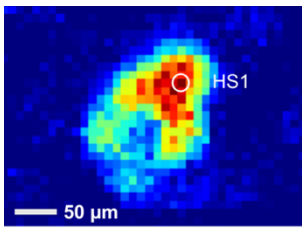

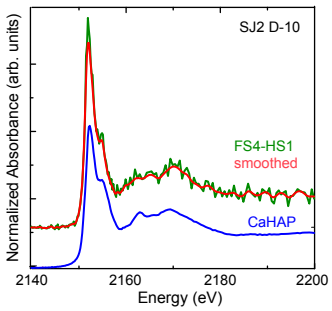

Figure 3. Representative phosphorus K-edge μ-XRF maps and μ-XANES (spot size ~5 μm) of airborne particles on filters compared with reference spectra deoxyribonucleic acid (DNA), PO_4 adsorbed on gibbsite (PO_4-gibbsite), and Ca hydroxyapatite (CaHAP). A. High elevation CO sample LS2 S-10; B. High elevation CA sample SH2 S-10; linear combination fit (in black) of two reference spectra (DNA and inositol hexakisphosphate (IHP)) shown for hot spot 2 (HS2); C. Low elevation CA sample SJ2 D-10; raw (green) and smoothed (red) spectra compared with reference spectrum Ca hydroxyapatite (CaHAP).

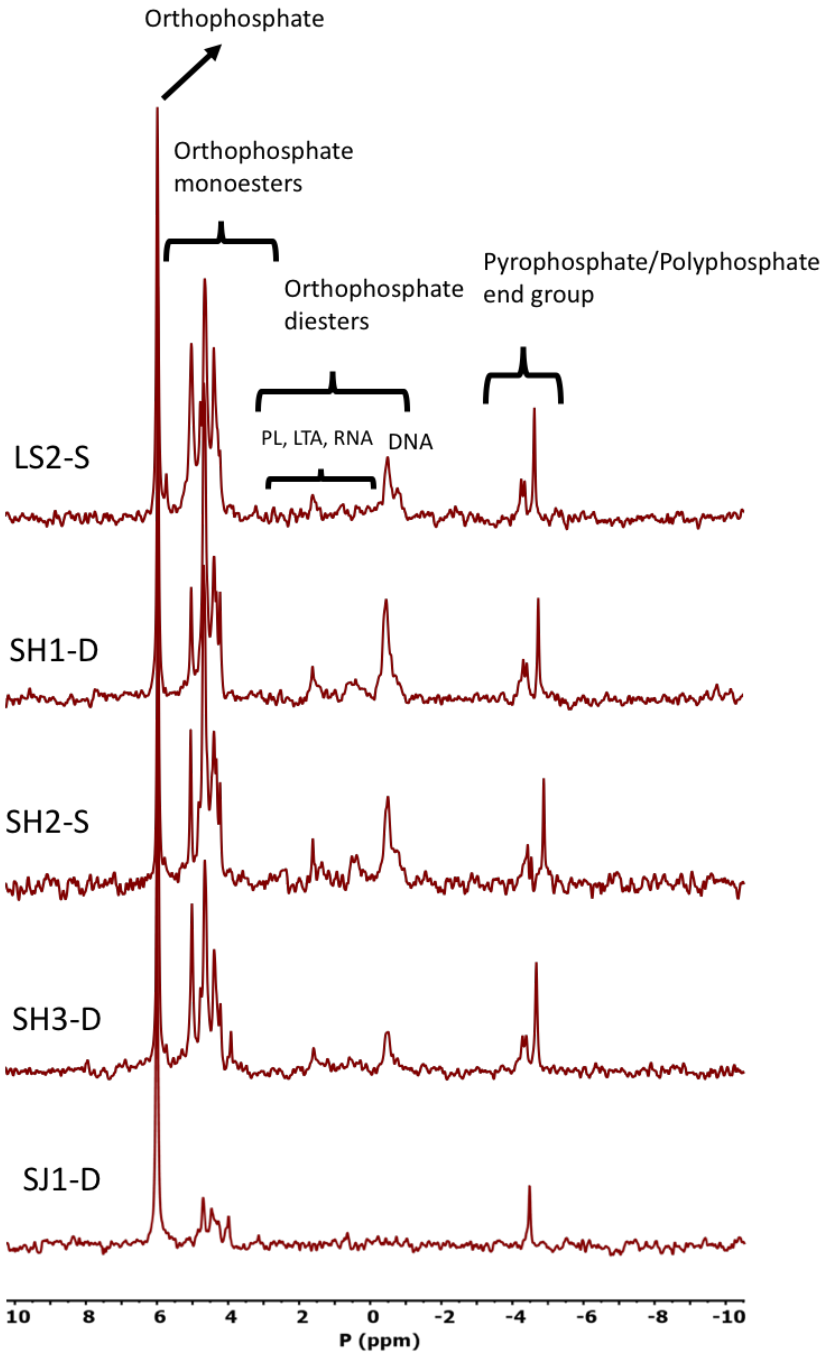

Figure 4. ^{31}P solution NMR spectra of extracted PM from high elevation CO (LS2-S) and CA (SH) sites compared with the low elevation CA site (SJ1-D). PL: phospholipids; LTA: lipoteichoic acid; RNA: ribonucleic acid; and DNA: deoxyribonucleic acid. See Table 1 for estimates of relative fractions of P species from peak area integration and Table S3 for peak assignments.

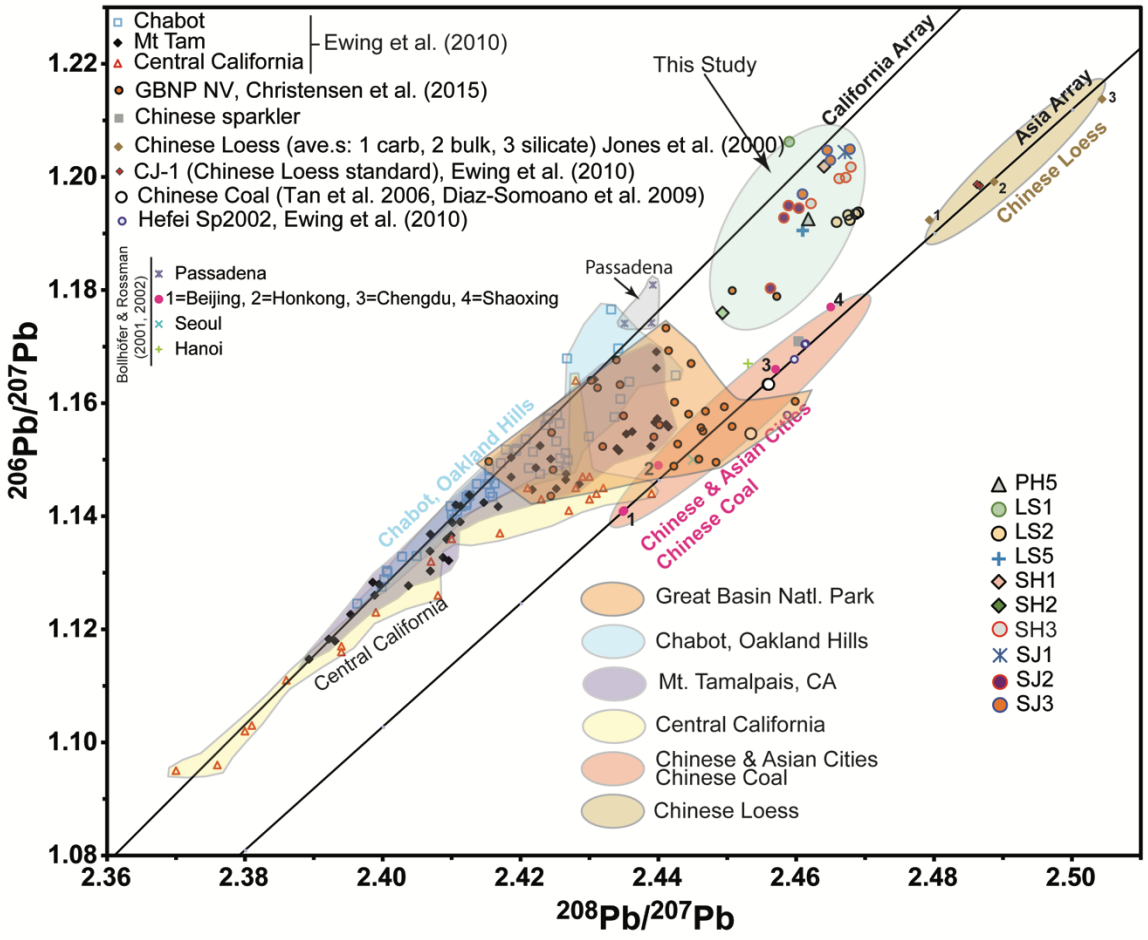

Figure 5. Lead (Pb) isotope ratios of particulate matter samples (from individual filters) compared with samples from prior studies of airborne particles from the western U.S. and sources in China. This study: LS, PH – high elevation CO-ERW; SH – high elevation CA-SSCZO; SJ – low elevation CA-SSCZO. Published studies: Ewing et al.[34]; Christensen et al.[35]; Jones et al.[65]; Tan et al.[66]; and Diaz-Somoano et al.[67]. See Table S4 for numerical results.

Table 1. Percentage of total extracted phosphorus (P) from NaOH-EDTA extraction and proportion of P species in extracted solutions estimated from integration and correction of NMR peaks.

Sample*	Extracted P† (% of total)	Inorganic P (%)	Organic P (%)	Monoester (%)	Diester (%)	Monoester/ Diester	Monoester‡ (corrected %)	Diester‡ (corrected %)	Monoester/ Diester (corrected)
LS2-S	80	25.4	74.6	60.2	14.4	4.2	27.3	47.3	0.58
SH1-D	85	26.4	73.6	53.3	20.3	2.6	22.6	51.0	0.44
SH2-S	89	22.3	77.7	57.7	20.0	2.9	27.9	49.8	0.56
SH3-D	89	33.5	66.5	56.1	10.4	5.4	19.4	47.1	0.41
SJ1-D	51	67.7	32.3	31.1	1.20	26	21.3	11.0	1.9

* Samples composited from multiple 10 µm filters to obtain 30-70 mg dry mass; D: Dry, S: Snow.
† Determined by digestion of total sample and residue after NaOH-EDTA extraction, and analysis of total P by ICP-OES.
‡ Estimated fractions corrected for degradation of diester phospholipid compounds to monoester α- and β- glycerophosphate.

Phosphorus Speciation in Atmospherically Deposited Particulate Matter and Implications for Terrestrial Ecosystem Productivity

Peggy A. O'Day[a,*,‡], Ugwumsinachi G. Nwosu[a,‡], Morgan Barnes[b], Stephen C. Hart[a], Asmeret Asefaw Berhe[a], John N. Christensen[c], and Kenneth H. Williams[c,d]

[a] Life and Environmental Sciences Department, and the Sierra Nevada Research Institute, University of California, Merced, CA 95343

[b] Environmental Systems Graduate Group, University of California, Merced, CA 95343

[c] Earth and Environmental Sciences, Lawrence Berkeley National Laboratory, Berkeley, CA 94720

[d] Rocky Mountain Biological Lab, Gothic, CO 81225

[*] correspondence to: poday@ucmerced.edu

[‡]These authors contributed equally

Supporting Information:

Pages: 19
Supplementary text: DETAILED MATERIALS AND METHODS
Figures S1 to S7
Tables S1 to S4
SI References

DETAILED MATERIALS AND METHODS

Sample Collection

Airborne particulate matter (PM) was collected at the East River Watershed, Colorado (CO-ERW) and the California Southern Sierra Critical Zone Observatory (CA-SSCZO) (Fig. S1). Locations and sample collection dates are shown in Table S1. Two high elevation sites at CO-ERW (LS and PH) were sampled by dry deposition (Sept.-Oct. 2016) and by snow sampling (winter, 2017). At the CA-SSCZO, the high elevation site (SH) was sampled twice by dry deposition (Sept.-Nov. 2016; July-Sept. 2017) and once by snow sampling (winter, 2017). The low elevation site CA-SSCZO (SJ) was below the snow line and was sampled three times by dry deposition (Table S1). Sample collection methods for dry deposition were previously employed by Aciego et al.[1] and used acid-cleaned passive collectors (25.4 cm diameter Teflon-coated pans) filled with quartz beads on top of a Teflon or polypropylene mesh at the base of the pan. Bird repellent and netting was used to protect from contamination. Multiple collectors (6 collectors per site) were deployed on two-meter high wooden poles at each site for 1-2 months. Pans were retrieved, washed with deionized (DI) water, and filtered in series with multiple 10 μm (PM ≥ 10 μm) and 1 μm (PM 1–10 μm) PTFE filters (for one sample, SJ1, 0.2 μm filters were used instead of 1 μm filter). Both individual and composited filters were analyzed, depending on the type of measurement.

Snow samples were collected at the three high elevation sites in spring or summer 2017 to capture PM deposition over the winter (Table S1). At the CO-ERW sites, snow samples were collected over the upper 10 cm of a 10,000 cm^2 snow field surface having visible accumulation of an outcropping dust layer, with the melted snow water then homogenized. At the high elevation CA-SSCZO site, a profile area (65 x 43 cm) was collected over a total snow depth of 134 cm. Samples were collected in approximately 20 cm increments with depth. The bottom 10 cm at the soil-snow interface were not collected to prevent contamination from the soil surface. A total of six layers were collected; this study focused on a sample (SH2) collected from the uppermost layer (0-20 cm).



Figure S1. Location of study sites in Colorado and California for airborne particulate matter collection. Inset photos show passive samplers for dry deposition collection.

Table S1. Summary of particulate matter sample locations and sampling periods for this study.

Site	Sample Type	Elevation (m)	Location	Collection Period
East River Watershed (ERW), Colorado				
LS1	Dry	3100	38°57'23.2"N, 107°01'43.9"W	09/17/16 – 10/30/16
LS2	Snow	3100	38°57'23.2"N, 107°01'43.9"W	07/10/17
PH1	Dry	2800	38°55'13.2"N, 106°56'57.0"W	09/17/16 – 10/30/16
PH2	Snow	2800	38°55'13.2"N, 106°56'57.0"W	04/17/17
Southern Sierra Critical Zone Observatory (SSCZO), California				
SH1	Dry	2700	37°04'01.4"N, 118°59'13.9"W	09/02/16 – 11/06/16
SH2	Snow	2500	37°01'31.2"N, 118°59'48.4"W	04/30/17
SH3	Dry	2700	37°04'01.4"N, 118°59'13.9"W	07/03/17 – 09/03/17
SJ1	Dry	400	37°06'28.7"N, 119°43'54.8"W	09/02/16 – 10/13/16
SJ2	Dry	400	37°06'15.2"N, 119°43'15.8"W	06/15/17 – 07/21/17
SJ3	Dry	400	37°06'15.2"N, 119°43'15.8"W	08/03/17 – 08/31/17

Elemental Analysis

All laboratory procedures used ultrapure water (18.2 MΩ·cm, EASYpure UV, Barnstead Thermolyne). Elemental sample composition was determined by acid digestion of PM samples and analysis using ICP-OES. Samples were digested using microwave acid digestion (Anton Paar Multiwave 3000) with aqua regia (9 mL HCl and 3 mL HNO_3 to 10-20 mg of dried sample). Digests were diluted with ultrapure water to 4% nitric acid prior to analysis. Samples were measured for total P, Ca, Mg, K, Al, and Fe by ICP-OES (PerkinElmer Optima 5300 DV). Acid blanks and standards of known concentrations were run repeatedly to ensure accuracy and reproducibility. Instrumental error (relative standard deviation) was ≤ 3%. For total P, the instrumental detection limit was 10 ppb. Results of bulk PM sample analyses are shown in Fig. S2 and S3.

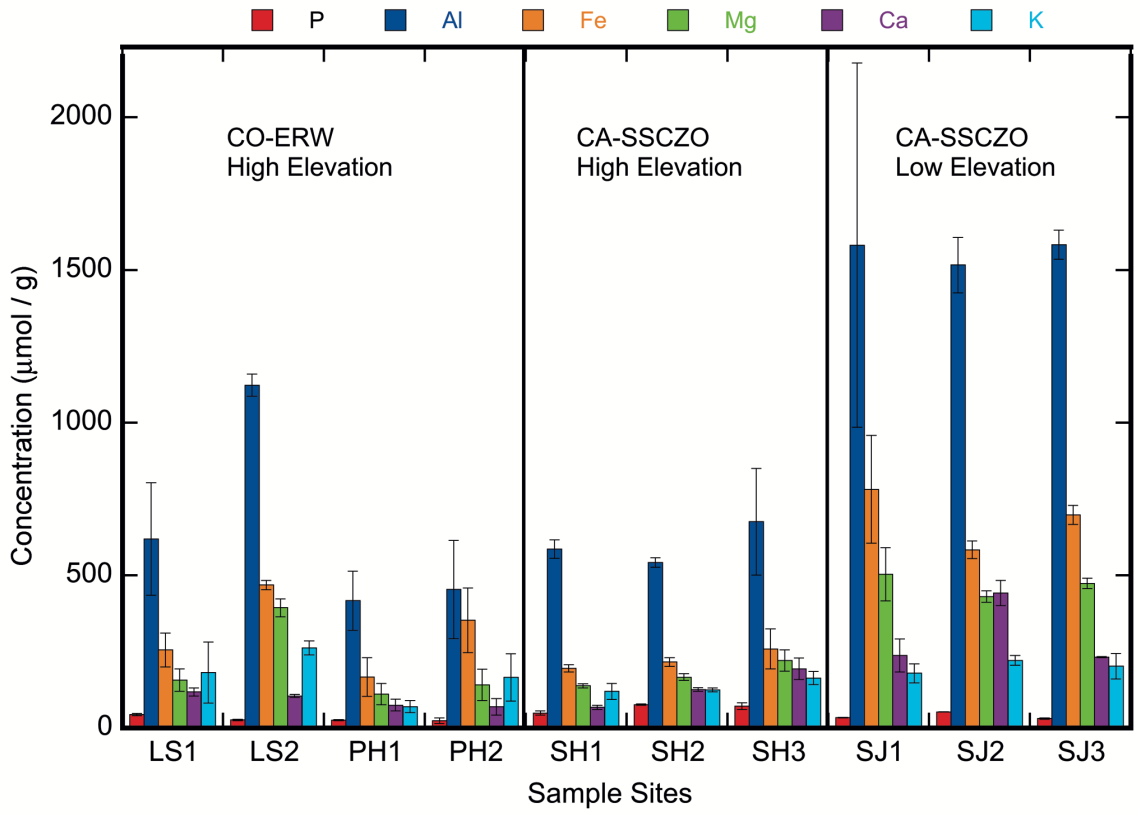

Figure S2. Elemental analysis of bulk PM samples from the Colorado East River Watershed, (CO-ERW) (LS1, LS2, PH1, PH2) the California Southern Sierra Critical Zone Observatory (CA-SSCZO) with high (SH1, SH2, SH3) and low (SJ1, SJ2, SJ3) elevation sites. Error bars are standard deviations of replicate analyses of different filter samples (n = 3 to 6).

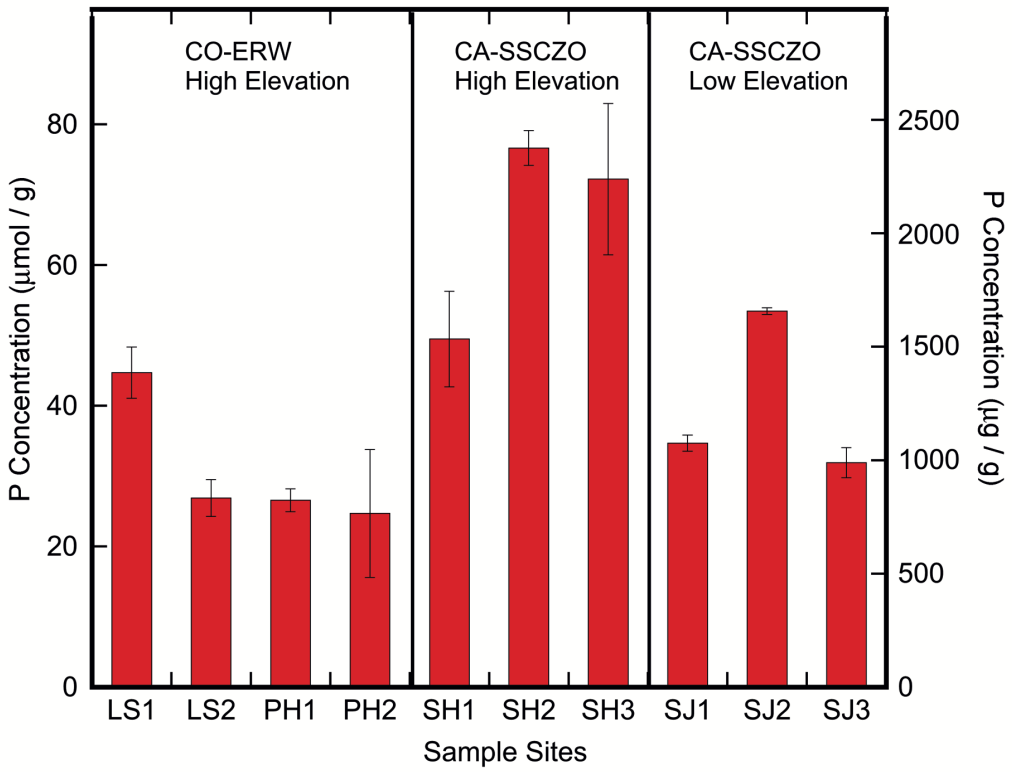

Figure S3. Total P concentrations (expanded from Fig. S2) in bulk PM samples from the Colorado East River Watershed, (CO-ERW) (LS1, LS2, PH1, PH2) the California Southern Sierra Critical Zone Observatory (CA-SSCZO) with high (SH1, SH2, SH3) and low (SJ1, SJ2, SJ3) elevation sites. Error bars are standard deviations of replicate analyses of different filter samples (n = 3 to 5).

Phosphorus K-edge X-ray Absorption Spectroscopy (XAS)

Phosphorus Reference Compounds

Phosphorus compounds were obtained from Sigma Aldrich (reagent grade or better). Phytate compounds (Al-, Ca-, and Fe-phytate) were synthesized in the laboratory according to a published method.[2] Gibbsite ($Al(OH)_3$) was obtained from Huber Engineered Materials (Micral 916). Ferrihydrite (amorphous $Fe(OH)_3$) and goethite (FeOOH) were synthesized in the laboratory following published methods.[3] Reference standards of dissolved orthophosphate or inositol hexakisphosphate (IHP) adsorbed on ferrihydrite, goethite, or gibbsite were prepared by shaking 30 ml of 2 mM of KH_2PO_4 or IHP solution in 0.01 KCl with 100 mg of adsorbent material for 18 h (pH ~6). For DNA adsorption on gibbsite, ~100 mg DNA was used in 30 ml of DI water. After the reaction period, suspensions were centrifuged at 16,500 rpm, supernatant solutions removed, and solid material dried at 45° C for 3 days, except for orthophosphate adsorbed on ferrihydrite and goethite reference standards, which were air dried for 4 days.

Bulk K-Edge Absorption Near-edge Structure (XANES) Spectroscopy

Bulk K-edge P-XANES were collected at beamline 14-3 at the Stanford Synchrotron Radiation Lightsource (SSRL), Stanford, CA and at the soft X-ray micro-characterization beamline (SXRMB) at the Canadian Light Source (CLS), Saskatoon, Canada. Sample spectra were collected by mounting PM filters directly on P-free, double-sided carbon tape. Reference compounds were diluted with either sugar or BN and mounted on sample holders with P-free, double-sided carbon tape. Reference compound spectra were monitored for self-absorption; fluorescence spectra for a few compounds were compared with spectra collected using a total electron yield (TEY) detector to verify no significant self-absorption the fluorescence signal. All spectra were collected at room temperature. At SSRL, storage ring energy was 3 GeV and beam current was 500 mA. Beamline 14-3 was equipped with a water-cooled Si(111) double-crystal monochromator (theta = 90^0 cut) and beamline energy resolution of ~1 x 10^{-4} eV. Samples were maintained in a He gas environment during data collection. XANES data were collected in fluorescence mode with a 4-channel Ge vortex detector. The storage ring at CLS was 2.9 GeV with maximum beam current of 250 mA. The SXRMB beamline was equipped with a Si (111) double-crystal monochromator. Samples were maintained in vacuum during data collection. Energy was calibrated at the P K-edge using either a NaH_2PO_4 standard, for which peak

maximum absorption was set to 2152.6 eV, or tetraphenylphosphonium bromide (PPh_4Br), with the first peak maximum set to 2146.96 eV. Lecithin was used as a secondary standard for energy calibration. Standard spectra were collected for each run and cross-calibrated between different beamlines and runs. At least 4 scans were collected for P reference standards and 8-16 scans for PM samples, and no changes in spectral features were observed in successive scans. XANES spectra were averaged and processed using Sam's Interface for XAS Package (SIXPACK).[4] Data processing and analyses were done with the ATHENA software package. (Demeter 0.9.20)[5] All of the P reference spectra shown in Fig. S4 were tested in linear combination fits (LCFs). Fits were performed with the component sum not forced to unity and only fits within 100 ± 2.5% were accepted. A series of sensitivity tests were performed by examining linear combinations of 1 to 4 reference compound spectra and ranked by statistical best fit (using ATHENA). The LCF with the highest rank using the fewest number of components, and with a component total of 100 ± 2.5%, was selected as the best fit. Numerical results are given in Table S2.

Microfocused (μ-) X-ray Fluorescence (XRF) and XANES

Microfocused synchrotron X-ray data were collected at both beamline 14-3 at SSRL and SXRMB at CLS under ring and beamline conditions given above. Particles spread on tape or filters were mapped at the P K-edge by μ-XRF with a 10 μm beam spot and μ-XANES spectra were collected on high count spots. Spot scans were averaged, processed, and analyzed by LCF in the same manner as described above for bulk sample spectra. Data were analyzed using Sam's Microprobe Analysis Kit (SMAK).

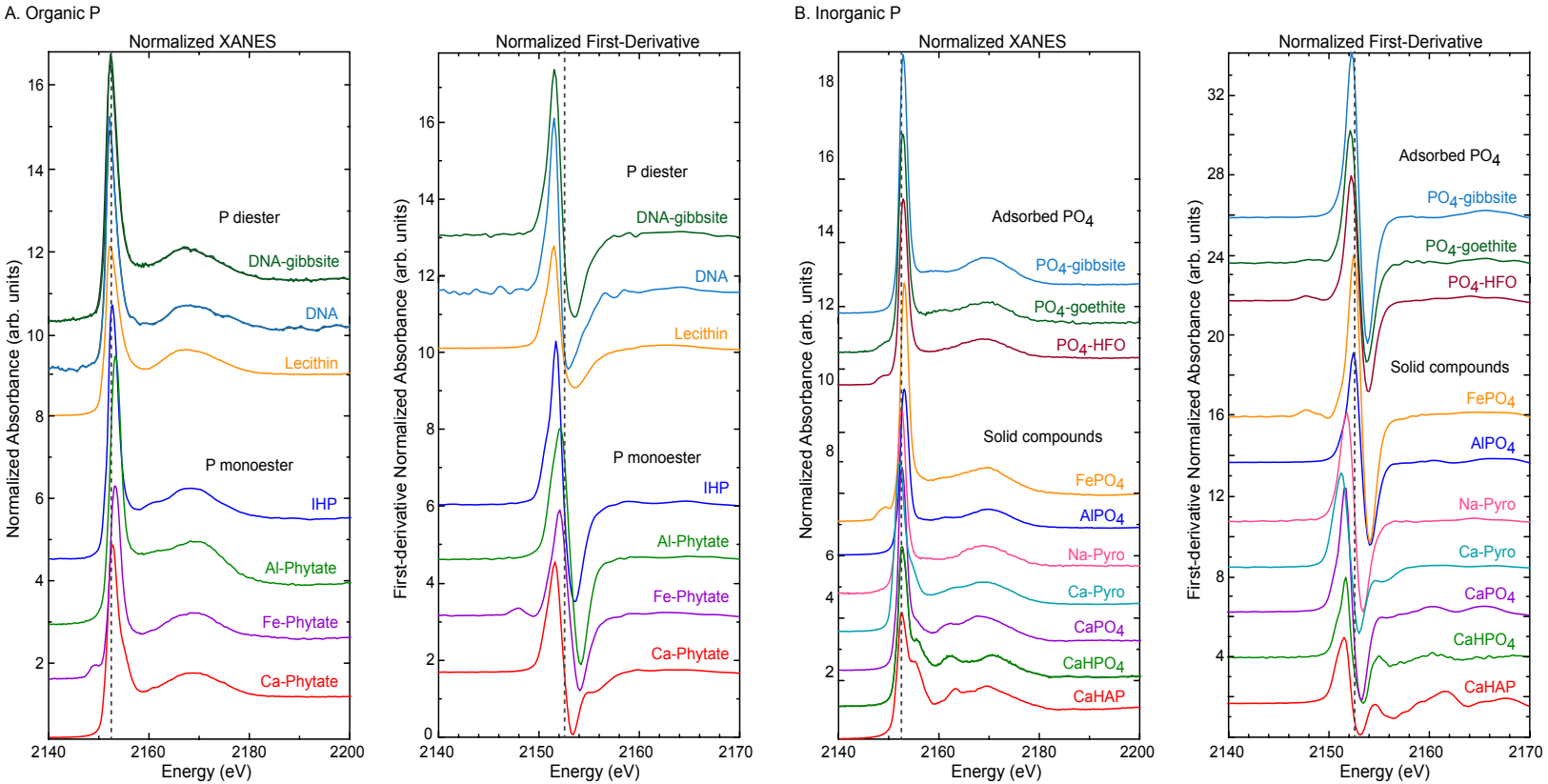

Figure S4. Phosphorus K-edge normalized and first-derivative XANES reference spectra. A. Organic P compounds and adsorbed species: Orthophosphate monoester (P-monoester) spectra: Ca-phytate, Fe-phytate, Al-phytate, IHP (inositol hexakisphosphate, Na salt); orthophosphate diester (P-diester) spectra: Lecithin ($C_{35}H_{66}NO_7P$), DNA (deoxyribonucleic acid), and DNA adsorbed on gibbsite (DNA-gibbsite). B. Inorganic orthophosphate compounds and adsorbed orthophosphate species (PO_4): Ca hydroxyapatite (Ca HAP), Ca hydrogen phosphate ($CaHPO_4$), $AlPO_4$, and $FePO_4$; PO_4 adsorbed on: hydrous ferric oxide (PO_4-HFO); goethite (FeOOH; PO_4-goethite), and gibbsite ($Al(OH)_3$; PO_4-gibbsite). Vertical dashed line indicates energy calibration using NaH_2PO_4 standard with peak maximum set to 2152.6 eV.

Analysis of Reference XANES spectra

Reference standards used for P K-edge XAS are shown in Fig. S4. Although P XANES reference spectra have generally similar features, differences in the energy and width of the sharp absorption maximum (2151.8-2153.5 eV), and in the shape and position of absorption features in the pre-edge (2148.5-2150.5 eV) and post-edge regions (2158-2170 eV) enable differentiation of different classes of compounds. Organic-P compounds were grouped as either monoester IHP (as inositol hexakisphosphate, Na salt) or diester (as DNA) forms. For DNA, spectra were collected for both the pure compound and as adsorbed species on gibbsite. Spectra of organic-P compounds showed a slight shift or broadening, or both, of the absorption maximum to lower energy relative to inorganic phosphate compound spectra. Spectra of inorganic orthophosphate bonded to iron (Fe), either in a bulk compound or as an adsorbed species, have distinct pre-edge features, whereas orthophosphate compounds with calcium (Ca) or aluminum (Al), or orthophosphate adsorbed to Al-hydroxide ($Al(OH)_3$ as gibbsite), have characteristic post-edge absorption features (Fig. S4). Spectra of Ca hydroxyapatite (CaHAP) and calcium hydroxy phosphate ($CaHPO_4$) exhibited a shift of the absorption maximum to slightly lower energy compared to the other inorganic P spectra.

Previous studies have noted that different forms of organic P were generally similar in their X-ray absorption spectral signature and thus could not be easily distinguished, although some studies have discussed spectral differences.[6, 7] Comparison of the reference spectra show subtle but resolvable differences among different classes of organic P compounds, particularly between P monoester and diester linkages, and among P monoester (phytate) bonded to metal cations. Different metal cations (particularly Ca^{2+}, Al^{3+}, or Fe^{3+}) have different electron-withdrawing affinities for O ligands that bridge between P and the metal cation, which imparts a slightly different energy shift to the maximum absorption peak, as well as differences in pre-edge (for Fe^{3+}) and post-edge (for Ca^{2+}) absorption features (Fig. S4). Likewise for inorganic P compounds, characteristic post-edge spectral signatures for Ca-bearing apatite and phosphate phases make them easy to identify in mixtures, and the presence of Fe imparts a distinctive pre-edge feature.[7, 8]

Solution ^{31}P Nuclear Magnetic Resonance (NMR)

Sample extraction

Particles were washed from 10 μm PTFE filters with DI water. Multiple filters from the same sampling event were combined to achieve adequate mass. Particle masses ranging from 30-70 mg were extracted with 5 ml of 0.25 M NaOH and 0.05 M EDTA solution for 6 h. After extraction, the suspension was centrifuged for 30 min at 12,200 rpm (Eppendorf Centrifuge 5417C). The supernatant solution was then separated from the residue and filtered with a 0.45 μm syringe filter. To pre-concentrate the extract, the filtered solutions were frozen at –18 °C and lyophilized for 24 h. Freeze-dried particles were reconstituted to a 0.8-1.0 ml volume with 1 M NaOH, from which samples were prepared and immediately used for NMR analysis. Sample residues were acid digested and analyzed for total P by the methods described above to determine the amount of extracted P.

NMR data collection and analysis

For NMR data acquisition, 600 μl of the extracted, pre-concentrated sample were transferred into a 5 mm NMR tube containing a ~100 μl of D_2O and mixed. ^{31}P NMR data were acquired at 20 °C on a two-channel Agilent 500 MHz ProPulse500 NMR System with a One NMR Probe and a 96-Sample Robot, which operates at ^{31}P frequency of 202.4 MHz. Spectra were recorded under the following instrumental conditions and parameters; 45° pulse, 0.68 s acquisition time, 1 s pulse delay, and no proton decoupling. The instrument was continuously calibrated with an external standard (85% phosphoric acid) to 0 ppm to avoid instrumental drift. NMR peaks were identified by the combination of visual inspection and comparison to previous literature, as well as comparison with P standards collected in a similar solution matrix as the unknown sample. Standards (phosphonic acid, sodium phosphate, lecithin, DNA, and myo-IHP) were also collected individually and used to verify peak positions and chemical shifts. In addition, peaks assignments were further confirmed by spiking previously analyzed samples with orthophosphate and other P standards (Fig. S5). Upon spiking the samples with α- and β-glycerophosphate, myo-IHP, glucose 1-phosphate, and glucose 6-phosphate, peaks in the P monoester region were identified and in agreement with previously published chemical shifts.[9] Peak identifications by Cade-Menun[9] were used to assign peaks in instances where the species was not included in spiking experiments.

Peak assignments and chemical shifts for P compound classes are summarized in Table S3. Orthophosphate was set at 6 ppm. Orthophosphate monester peaks were identified between 5.75 and 3.15 ppm. Orthophosphate diester peaks with chemical shifts between ~ 2.46 to ~ 0.64 ppm were all assignable to phospholipids, lipoteichoic acid, and RNA. Chemical shifts for DNA peaks were identified at –0.29 to –0.65 ppm.[9] Another diester peak identified at –1.25 to –1.31 is believed to be associated with the DNA. After spiking, peaks identified at 5.06 to 5.10 ppm and 4.69 to 4.75 ppm were assignable to α- and β- glycerophosphate, which are known degradation products of phospholipids.[10, 11] Similarly, peaks at 5.75 to 5.82 ppm, 4.81 to 4.88 ppm, 4.44 to 4.47 ppm, and 4.27 to 4.30 ppm became evident as myo-IHP after spiking. Pyrophosphate peaks were identified at –4.45 to –4.55 ppm and were all associated with close doublet peaks (–4.08 to –4.12 and –4.18 to –4.21 ppm) assignable to the polyphosphate end groups. Other polyphosphate peaks occurred at –9.46 and between –18 to –19 ppm.

NMR spectra were processed (phased and baseline corrected) using the MestReNova 14.0.1 NMR software package. Following spiking experiments, visual identification, and comparison with published standards[9], peak regions were manually integrated to determine the relative percent of an identified species, and summed according to compound class. Error was determined from replicate runs on LS2-S samples using orthophosphate, orthophosphate monoester, DNA, and pyrophosphate/polyphosphate peaks, and was estimated to be ≤ 2.0%. Estimated fractions of total diester and monoester compounds were corrected for degradation of diester phospholipid compounds to monoester α- and β- glycerophosphate. These degradation peaks were identified by addition of the known compound, and peak areas in the unspiked NMR spectrum were manually subtracted from the monoester total and added to the diester total.[9, 12] No other peak corrections were done.

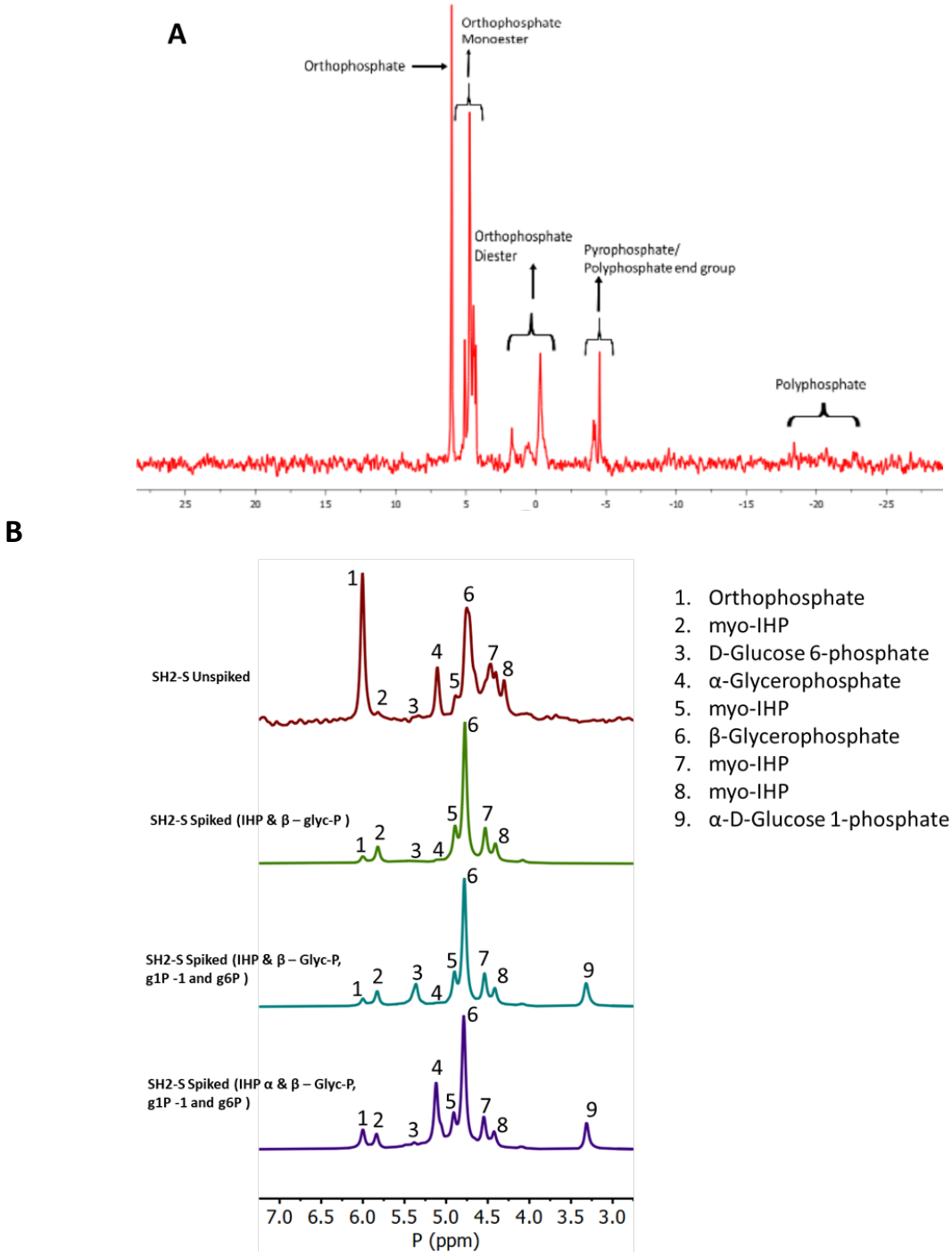

Figure S5. ^{31}P solution NMR spectra of extracted airborne particulate matter (PM) samples. A. Chemical shift regions of major P groups. B. Expanded spectra of chemical shift peaks as labeled in the P monoester region for CA-SSCZO SH2 PM sample before and after addition of standards: myo-IHP (inositol hexakisphosphate), D-glucose 6-phosphate, α-glycerol 6-phosphate, β-glycerophosphate, and α-D-glucose 1-phosphate.

Lead Isotopic Analysis

Lead isotopic analysis followed methods used by Ewing et al.[13], Christensen et al.[14], Pierce et al.[15], and Asher et al.[16] using a Neptune Plus (Thermo-Fisher) multi-collector ICP source mass spectrometer (MCICPMS) at Lawrence Berkeley National Laboratory (LBNL). Aliquots of solutions from samples dissolved for total element analysis were taken to provide 10-100 ng of Pb for isotopic analysis. The aliquots were dried down in Teflon vials (Savillex, LLC), brought up again in high purity 0.5 M HBr (Seastar Chemicals), and loaded on new AG1x8 resin (BioRad) using small Teflon columns. The columns were then eluted with 0.5 M HBr to strip matrix elements, and Pb collected off the columns with high purity 6 M HCl (Seastar Chemicals). The separated Pb was then dried down and taken up again in 1 ml 0.3 N HNO_3 (high purity, Seastar Chemicals) from which 10% by volume was taken for Pb concentration determination using the Neptune Plus MCICPMS. Based on this result, the remaining sample was spiked with natural Tl (NIST SRM997) at ~5 ng Tl per 25 ng sample Pb. The isotopic composition of the Tl-sample Pb mixture was measured on the Neptune Plus using the monitored $^{230}Tl/^{205}Tl$ ratio to correct $^{206}Pb/^{207}Pb$ and $^{208}Pb/^{206}Pb$ for instrumental mass fractionation correction, with normalization to the NIST SRM981 Pb isotopic standard spiked with Tl as above. Sample $^{206}Pb/^{207}Pb$ and $^{208}Pb/^{206}Pb$ were also corrected for total chemistry blank, which in most cases was less than 1% of sample Pb mass. Analytical uncertainties of the $^{206}Pb/^{207}Pb$ and $^{208}Pb/^{206}Pb$ ratios were better than ±0.01 ‰ (2σ) based on replicates of SRM981.

Calculation of the Fraction of Asian Pb

The measured $^{206}Pb/^{207}Pb$ and $^{208}Pb/^{206}Pb$ of the PM samples were used to calculate the fraction of Asian Pb in the sample using a mixing model presented by Ewing et al.[13] (cf.[14-16]). First, the parameter $\Delta 208Pb_{smpl}$ is calculated, which represents the horizontal displacement of the sample from the California Pb isotope data array shown in Fig. S5 using Eq. A:

$$\Delta^{208}Pb_{smpl} = 1000[(^{208}Pb/^{207}Pb)_{smpl} - (^{208}Pb/^{207}Pb)_{CA}] \qquad \text{Eq. A}$$

where $(^{208}Pb/^{207}Pb)_{CA}$ is the ratio the sample would have if its measured $^{206}Pb/^{207}Pb$ is plotted on the California array[13] The fraction of Asian Pb in a sample ($F_{AsianPb}$) is then calculated from Eq. B:

$$F_{Asia}Pb = \Delta^{208}Pb_{smpl}/\Delta^{208}Pb_{Asia} \qquad \text{Eq. B}$$

where $\Delta^{208}Pb_{Asia}$ represents the horizontal offset of Asian sources from the California array; for 100% Asian Pb the threshold value is 25. For samples with $\Delta^{208}Pb_{smpl}$ equal to zero (or less), the sample plots on the California array (or to the left of it) and the fraction of Asian Pb is taken as zero.

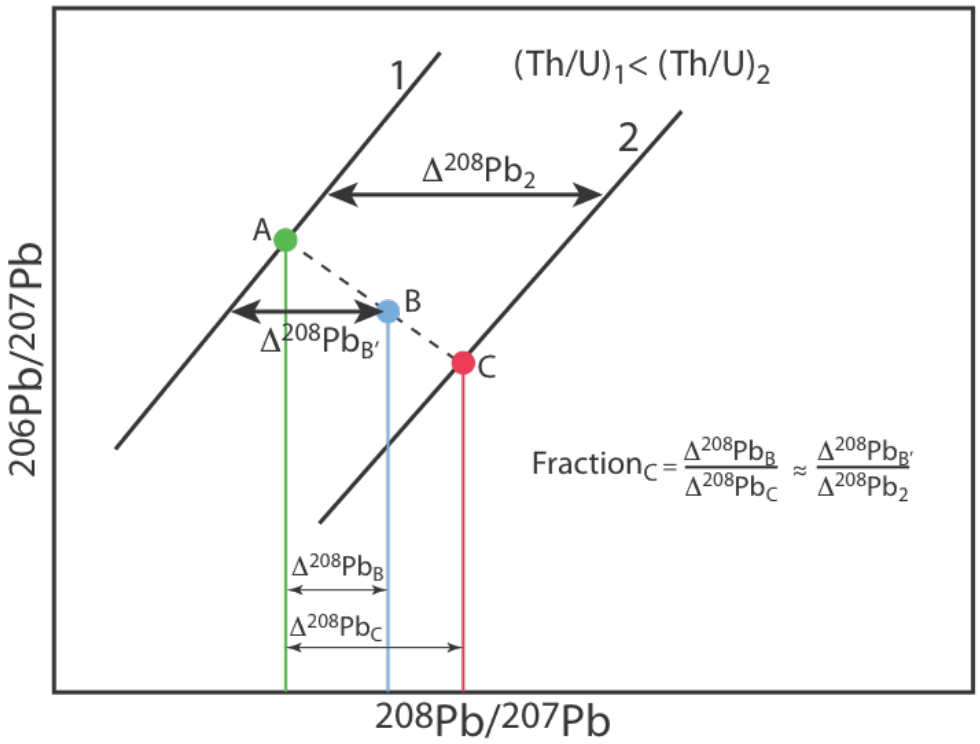

Figure S6. A schematic illustrating the calculation of the fraction of Asian Pb in a sample.

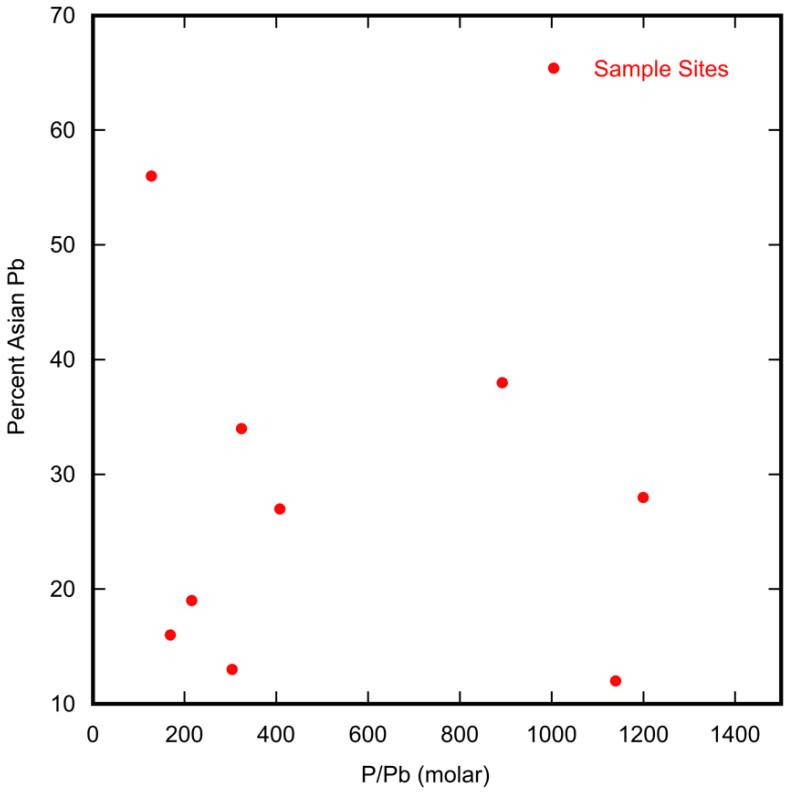

Figure S7. Percent Asian Pb calculated from Pb isotopic analyses (Table S4) compared to the molar ratio of total P/Pb in digested PM samples. Each point is an average of measurements (n = 1 to 5) for each sample site.

Table S2. Results of linear combination fits of bulk XANES spectra of particulate matter samples.

		Organic P (%)			Inorganic P (%)				Inorganic P (adsorbed) (%)			
Sample*	**Filter size† (μm)**	**Mono-ester (IHP)**	**Diester (DNA)**	**Diester adsorbed (DNA/ gibbs)**	**Ca HAP**	**$CaHPO_4$**	**$AlPO_4$**	**$FePO_4$**	**$–PO_4$/ gibbs**	**$–PO_4$/ goeth**	**Total**	**R-factor ($x10^{-4}$)‡**
LS1-D	10	21.0		54.3			13.3		9.7		98.3	2.68
LS2-S	10	33.8		32.6		6.5	29.5				102.4	3.22
LS2-S	1	55.9	15.0				29.1				100.0	4.29
PH1-D	10	32.4		59.8					6.9		99.1	5.23
PH2-S	10			76.9	5.9				16.8		99.6	1.81
PH2-S	1	35.3	20.3	38.9					5.8		100.3	6.31
SH1-D	10	13.9	23.2	53.5					9.3		99.9	6.55
SH2-S	10	22.0		71.0					6.9		99.9	6.68
SH2-S	1	59.2		40.4							99.6	10.3
SH3-D	10	14.5		65.8	8.5				11.3		100.1	10.9
SH3-D	1	27.9		72.0							99.9	18.4
SJ1-D	10	44.1	11.9		27.3		16.7				100.0	6.41
SJ1-D	0.2	26.4			57.2				18.6		102.2	6.45
SJ2-D	10	24.4	29.4		33.4				12.5		99.7	11.2
SJ2-D	1	40.6	37.2			12.3			10.1		100.2	18.5
SJ3-D	10		30.2		28.3				16.4	25.4	100.3	10.0
SJ3-D	1		18.9		18.6			15.6		46.2	99.3	15.1

* D: Dry, S: Snow. Blank cells indicate that the component was not identified in linear combination fit.
† Individual filters with PM measured directly in the beam.
‡ R-factor: statistical goodness-of-fit equal to ($\sum$ (data-fit)^2 / $\sum$ (data)^2)

Table S3. ^{31}P NMR chemical shift assignments in ppm.

Sample*	Ortho-P†	Phosphorus Monoesters‡						Phosphorus Diesters§		PyroP¶	PolyP#
		myo-IHP	g6P	P-chol	g1P	α-Glyc	β-Glyc	DNA	Other Diesters		
LS2-S	6.00	5.75, 4.81, 4.44, 4.27	5.38	3.98	3.27	5.06	4.69	-0.38, -0.65	1.70, 0.85	-4.45	-4.09 , -4.18 -18.04, -18.20, -18.32
SH1-D	6.00	5.79, 4.85, 4.44, 4.28	5.37	4.05	3.19	5.08	4.73	-0.32	1.72, 0.66, -1.25	-4.53	-4.12, - 4.21, -9.46 -18.32, -18.41, -18.50
SH2-S	6.00	5.82, 4.88, 4.47, 4.30	5.32	4.03		5.10	4.75	-0.29, -0.53	2.46, 1.76, 0.69, -1.31	-4.55	-4.11, -4.21
SH3-D	6.00	5.77, 4.82, 4.45, 4.27	5.33	3.98		5.06	4.71	-0.32, -0.62	1.70, 0.71	-4.46	-4.08, -4.18
SJ1-D	6.00	5.77, 4.84, 4.47, 4.28			3.15	5.08	4.70		0.99, 0.64	-4.50	

* D: Dry, S: Snow.
† Ortho-P: orthophosphate assigned to 6 ppm.
‡ myo-IHP: myo-inositol hexakisphosphate; g6p: glucose 6-phosphate; P-chol: phosphocholine; g1P: glucose 1-phosphate. α-Glyc and β-Glyc: α- and β- glycerophosphate originated from the degradation of phospholipids as confirmed by spiking.
§ DNA: deoxyribonucleic acid. Other diesters were PL: phospholipids; LTA: lipoteichoic acid; RNA: ribonucleic acid; and other unknown peaks at -1.25, -1.31, and 2.46 ppm for SH1-D and SH2-S.
¶ PyroP: pyrophosphates.
# PolyP: polyphosphates.

Table S4. Total Pb concentrations, standard deviations, and isotope ratios of particulate matter samples, and estimated percent sourced from Asia.

Sample*	Sample ID	Pb (mg kg^{-1})	$^{206}Pb/^{207}Pb$	$\pm 2\sigma$	$^{208}Pb/^{206}Pb$	$\pm 2\sigma$	Percent Asian Source
LS1-D	LS1016 5	45.3	1.206227	3.1E-05	2.458998	8.2E-05	0%
LS1-D	LS5	40.8	1.190526	1.8E-05	2.460943	4.7E-05	37%
LS2-S	LSO717 3	49.0	1.193270	3.0E-05	2.467513	6.8E-05	54%
LS2-S	LS0717 21	41.3	1.193749	3.0E-05	2.469005	6.3E-05	59%
LS2-S	LS0717 15	43.6	1.193455	3.0E-05	2.468631	6.0E-05	58%
LS2-S	LS0717 10	40.5	1.192018	3.1E-05	2.465858	6.5E-05	52%
LS2-S	LS0717 16	44.3	1.192371	3.0E-05	2.467785	6.5E-05	58.5%
PH1-D	PH5	17	1.192554	2.6E-05	2.461752	8.1E-05	34%
SH1-D	SH4A	9	1.201856	1.9E-05	2.464025	3.4E-05	12%
SH2-S	SH-SW5	17.8	1.175955	1.7E-05	2.449306	5.0E-05	38%
SH3-D	SH 9/3/17 #3	15.1	1.199895	1.4E-05	2.467068	3.8E-05	31%
SH3-D	SH 9/3/17 #9	11.3	1.195286	1.1E-01	2.462015	3.4E-05	26%
SH3-D	SH 9/3/17 #10	11.7	1.201739	1.4E-05	2.467807	4.2E-05	28%
SH3-D	SH 9/3/17 #11	11.8	1.199707	1.2E-05	2.466107	2.6E-05	28%
SJ1-D	SJER	42.6	1.204379	3.7E-05	2.467054	1.42E-04	16%
SJ2-S	10SJ0717 3	26.1	1.194487	2.9E-05	2.460384	5.4E-05	22%
SJ2-S	10SJ0717 4a	25.5	1.194937	2.9E-05	2.458881	5.5E-05	14%
SJ2-S	10SJ0717 5	24.2	1.192785	3.0E-05	2.458207	5.4E-05	19%
SJ2-S	10SJ0717 7	33.0	1.180319	2.9E-05	2.456263	5.6E-05	52%
SJ3-D	10SJO817 1	25.4	1.196959	3.0E-05	2.460900	6.4E-05	16%
SJ3-D	10SJO817 #4b	22.5	1.204906	3.1E-05	2.467791	5.7E-05	17%
SJ3-D	10SJO817 #6	17.6	1.202942	1.4E-05	2.464961	4.0E-05	12.5%
SJ3-D	10SJO817 #7	21.6	1.204707	1.5E-05	2.464490	4.1E-05	5%

*Individual filter samples were measured for a given sample location and sampling interval; D: Dry, S: Snow

SI References

(1) Aciego, S. M.; Riebe, C. S.; Hart, S. C.; Blakowski, M. A.; Carey, C. J.; Aarons, S. M.; Dove, N. C.; Botthoff, J. K.; Sims, K. W. W.; Aronson, E. L., Dust outpaces bedrock in nutrient supply to montane forest ecosystems. *Nature Comm.* **2017,** *8*, 10.

(2) He, Z.; Honeycutt, C. W.; Zhang, T.; Bertsch, P. M., Preparation and FT-IR characterization of metal phytate compounds. *J. Environ. Qual.* **2006,** *35*, (4), 1319-1328.

(3) Schwertmann, U.; Cornell, R. M., *Iron Oxides in the Laboratory: Preparation and Characterization, Second Edition*. Wiley-VCH: 2000.

(4) Webb, S. M., SIXpack: a graphical user interface for XAS analysis using IFEFFIT. *Phys. Scr.* **2005,** *T115*, 1011-1014.

(5) Ravel, B.; Newville, M., "ATHENA, ARTEMIS, HEPHAESTUS: Data analysis for X-ray absorption spectroscopy using IFEFFIT" *J. Synch. Rad.* **2005**, 537-541.

(6) Hesterberg, D., Chapter 11 - Macroscale Chemical Properties and X-Ray Absorption Spectroscopy of Soil Phosphorus. In *Developments in Soil Science*, Balwant, S.; Markus, G., Eds. Elsevier: 2010; Vol. Volume 34, pp 313-356.

(7) Prietzel, J.; Harrington, G.; Hausler, W.; Heister, K.; Werner, F.; Klysubun, W., Reference spectra of important adsorbed organic and inorganic phosphate binding forms for soil P speciation using synchrotron-based K-edge XANES spectroscopy. *J. Synch. Rad.* **2016,** *23*, (2), 532-544.

(8) Khare, N.; Hesterberg, D.; Martin, J. D., XANES investigation of phosphate sorption in single and binary systems of iron and aluminum oxide minerals. *Environ. Sci. Technol.* **2005,** *39*, (7), 2152-2160.

(9) Cade-Menun, B. J., Improved peak identification in P-31-NMR spectra of environmental samples with a standardized method and peak library. *Geoderma* **2015,** *257*, 102-114.

(10) Turner, B. L.; Mahieu, N.; Condron, L. M., Phosphorus-31 nuclear magnetic resonance spectral assignments of phosphorus compounds in soil NaOH-EDTA extracts. *Soil Sci. Soc. Am. J.* **2003,** *67*, (2), 497-510.

(11) Doolette, A. L.; Smernik, R. J.; Dougherty, W. J., Spiking Improved Solution Phosphorus-31 Nuclear Magnetic Resonance Identification of Soil Phosphorus Compounds. *Soil Sci. Soc. Am. J.* **2009,** *73*, (3), 919-927.

(12) Schneider, K. D.; Cade-Menun, B. J.; Lynch, D. H.; Voroney, R. P., Soil Phosphorus Forms from Organic and Conventional Forage Fields. *Soil Sci. Soc. Am. J.* **2016,** *80*, (2), 328-340.

(13) Ewing, S. A.; Christensen, J. N.; Brown, S. T.; Vancuren, R. A.; Cliff, S. S.; Depaolo, D. J., Pb Isotopes as an Indicator of the Asian Contribution to Particulate Air Pollution in Urban California. *Environ. Sci. Technol.* **2010,** *44*, (23), 8911-8916.

(14) Christensen, J. N.; Weiss-Penzias, P.; Fine, R.; McDade, C. E.; Trzepla, K.; Brown, S. T.; Gustin, M. S., Unraveling the sources of ground level ozone in the Intermountain Western United States using Pb isotopes. *Sci. Total Environ.* **2015,** *530*, 519-525.

(15) Pierce, A. M.; Gustin, M. S.; Christensen, J. N.; Loria-Salazar, S. M., Use of multiple tools including lead isotopes to decipher sources of ozone and reactive mercury to urban and rural locations in Nevada, USA. *Sci. Total Environ.* **2018,** *615*, 1411-1427.

(16) Asher, E. C.; Christensen, J. N.; Post, A.; Perry, K.; Cliff, S. S.; Zhao, Y. J.; Trousdell, J.; Faloona, I., The Transport of Asian Dust and Combustion Aerosols and Associated Ozone to North America as Observed From a Mountaintop Monitoring Site in the California Coast Range. *J. Geophys. Res., Atmos.* **2018,** *123*, (10), 5667-5680.